ELSEVIER

Physica A 258 (1998) 273–302

PHYSICA A

Image representation of a spherical particle near a hard wall

B. Cichocki [a,b], R.B. Jones [c,*]

[a] *Institute of Theoretical Physics, Warsaw University, Hoza 69, 00-618 Warsaw, Poland*

[b] *Institute of Fundamental Technological Research, Polish Academy of Sciences, Świętokrzyska 21, 00-049 Warsaw, Poland*

[c] *Department of Physics, Queen Mary and Westfield College, Mile End Road, London E1 4NS, UK*

Received 9 April 1998

Abstract

The motion of a spherical colloidal particle suspended in a moving fluid near a planar hard wall or free surface is considered. The particle types include hard spheres with mixed slip-stick boundary conditions, droplets with high surface tension and porous particles. A general expression for the flow field is obtained in terms of a set of force multipoles induced on the particle and on its mirror image in the bounding surface. An earlier calculation of the friction and mobility functions for the particle is extended to include coupling to an incident linear shear flow. A numerical representation of all these functions is given which is accurate at all separations of particle and boundary. These results are used to study the position and orientation of a hard sphere falling towards a wall under gravity in the presence of a shear flow. © 1998 Elsevier Science B.V. All rights reserved.

PACS: 82.70.Dd; 83.70.Hq; 83.10.Pp; 47.15.Gf

Keywords: Colloids; Suspensions; Stokes flow; Boundary flows; Image methods; Shear flow

1. Introduction

Colloidal dispersions of particles of sub-micron size are of great interest both for their technological applications and for their use as model systems in which many phenomena of statistical physics can be experimentally observed which would otherwise be unobservable in atomic or molecular systems with their much shorter time and length scales [1–5]. The transport properties of such dispersions are governed by the microhydrodynamics of the Stokes flow around the suspended particles [6], by the hard-sphere or electrostatic forces between the particles and by the thermal fluctuations of the

* Corresponding author. Tel.: +44 (0)171 975 5041; fax: +44 (0)181 981 9465; e-mail: r.b.jones@qmw.ac.uk.

0378-4371/98/$19.00 Copyright © 1998 Elsevier Science B.V. All rights reserved.
PII: S0378-4371(98)00267-2

suspending fluid which produce Brownian motion. For high density bulk suspensions of hard-sphere particles, powerful computer simulation techniques have made possible the study of particle diffusivities and the effective viscosity [7–9].

More recently there has been great interest in the properties of dispersions near a bounding wall or a fluid–fluid interface. Light-scattering studies and modern forms of microscopy can be used to study single particle motion near a boundary [10,11]. Problems of sedimentation [12], or re-suspension of sediments by a shear flow [13] or adsorption and escape of particles at a wall [14,15] all depend on the hydrodynamic flow around a particle near a wall. The analysis and study of such systems, especially by computer simulation, depends on an analysis of the force multipoles exerted on the fluid by the particle and on the Green tensor which propagates these multipoles between particles. Although the problem of a single hard-sphere near a hard wall is an old one [16], we have found a new representation of the Green tensor for this geometry which leads to a simplified image representation of the flow around any spherical particle near a hard wall. Such a representation is necessary for an efficient simulation study of many particles near such a wall [17].

Although we intend to use this new representation for the computer simulation of clusters of particles near a wall, it already gives useful results for the hydrodynamic properties of a single spherical particle moving near a hard wall or interface. In Section 2 we recall some general features of the one particle problem, in Section 3 we give the new representation of the Green tensor and use it to obtain a decomposition of the flow field expressed in terms of force multipoles on the sphere and its image. In Section 4 we give a simplified calculation of the grand resistance operator. We use this calculation in Section 5 to give explicit accurate analytic representations of the one particle friction functions. In Section 6 the mobility functions are obtained algebraically in terms of the friction functions. In Section 7 we look at a simple application to a sphere falling towards a wall in the presence of a shear flow and, finally, in Section 8 summarize our results.

2. Formulation of the one-sphere problem

We consider a spherically symmetric particle suspended in incompressible Newtonian liquid of shear viscosity η which is bounded by a planar hard wall. The Stokes flow around the particle is described by the linearized Navier–Stokes equations:

$$\eta\nabla^2\boldsymbol{v}(\boldsymbol{r}) - \nabla p(\boldsymbol{r}) = -\boldsymbol{F}(\boldsymbol{r}), \quad \nabla\cdot\boldsymbol{v}(\boldsymbol{r}) = 0\,, \tag{1}$$

where $\boldsymbol{v}(\boldsymbol{r})$ is the fluid velocity field, $p(\boldsymbol{r})$ is the pressure field and $\boldsymbol{F}(\boldsymbol{r})$ is the force density exerted on the fluid by the particle. This description uses the induced force picture of the particle [18–20] in which the fluid equations of motion (1) are extended to the interior of the particle which is replaced simply by an appropriate force density $\boldsymbol{F}(\boldsymbol{r})$. This picture is valid not only for hard spheres with mixed stick-slip boundary conditions at the surface, but also for spherical droplets and porous particles. Detailed

expressions for the force density for each type of particle may be found elsewhere [21].

We shall be interested in the case in which the sphere is subject to a general incident flow field $\boldsymbol{v}_0(\boldsymbol{r})$, $p_0(\boldsymbol{r})$ which, in the absence of the particle, obeys the homogeneous equations

$$\eta\nabla^2\boldsymbol{v}_0(\boldsymbol{r}) - \nabla p_0(\boldsymbol{r}) = 0, \qquad \nabla\cdot\boldsymbol{v}_0(\boldsymbol{r}) = 0\,, \tag{2}$$

and satisfies the hard wall boundary conditions. We can then write the solution to Eq. (1) as

$$\begin{aligned}\boldsymbol{v}(\boldsymbol{r}_1) &= \boldsymbol{v}_0(\boldsymbol{r}_1) + \boldsymbol{v}_1(\boldsymbol{r}_1) = \boldsymbol{v}_0(\boldsymbol{r}_1) + \int \boldsymbol{T}(\boldsymbol{r}_1,\boldsymbol{r}_2)\cdot\boldsymbol{F}(\boldsymbol{r}_2)\,d\boldsymbol{r}_2\,,\\ p(\boldsymbol{r}_1) &= p_0(\boldsymbol{r}_1) + p_1(\boldsymbol{r}_1) = p_0(\boldsymbol{r}_1) + \int \boldsymbol{Q}(\boldsymbol{r}_1,\boldsymbol{r}_2)\cdot\boldsymbol{F}(\boldsymbol{r}_2)\,d\boldsymbol{r}_2\,,\end{aligned} \tag{3}$$

where the Green tensor $\boldsymbol{T}$ and associated vector $\boldsymbol{Q}$ satisfy

$$\eta\nabla_1^2\boldsymbol{T}(\boldsymbol{r}_1,\boldsymbol{r}_2) - \nabla_1\boldsymbol{Q}(\boldsymbol{r}_1,\boldsymbol{r}_2) = -\mathbf{1}\delta(\boldsymbol{r}_1-\boldsymbol{r}_2), \qquad \nabla_1\cdot\boldsymbol{T}(\boldsymbol{r}_1,\boldsymbol{r}_2) = 0\,, \tag{4}$$

together with appropriate boundary conditions at the hard wall and at infinity. Here ∇_1^2 and ∇_1 denote the Laplacian and the gradient with respect to $\boldsymbol{r}_1$. By use of the Lorentz reciprocity theorem [23] one can show that $\boldsymbol{T}$ satisfies

$$T_{\alpha\beta}(\boldsymbol{r}_1,\boldsymbol{r}_2) = T_{\beta\alpha}(\boldsymbol{r}_2,\boldsymbol{r}_1)\,. \tag{5}$$

It can also be expressed in the form

$$\boldsymbol{T}(\boldsymbol{r}_1,\boldsymbol{r}_2) = \boldsymbol{T}_0(\boldsymbol{r}_1-\boldsymbol{r}_2) + \Delta\boldsymbol{T}(\boldsymbol{r}_1,\boldsymbol{r}_2)\,, \tag{6}$$

where $\boldsymbol{T}_0$ is the Oseen tensor, the Green tensor for unbounded fluid, and $\Delta\boldsymbol{T}$ is the correction arising from the presence of a boundary. The fundamental solution to Eq. (4) for unbounded fluid is explicitly

$$\boldsymbol{T}_0(\boldsymbol{x}) = \frac{1}{8\pi\eta x}(\mathbf{1}+\hat{\boldsymbol{x}}\hat{\boldsymbol{x}}), \qquad \boldsymbol{Q}_0(\boldsymbol{x}) = \frac{1}{4\pi x^2}\hat{\boldsymbol{x}}\,, \tag{7}$$

with $\boldsymbol{x} = \boldsymbol{r}_1 - \boldsymbol{r}_2$ and $\hat{\boldsymbol{x}} = \boldsymbol{x}/x$. In the decomposition (6) the singularity of the kernel $\boldsymbol{T}$ at $\boldsymbol{r}_1 = \boldsymbol{r}_2$ is contained in the Oseen tensor $\boldsymbol{T}_0$ while the correction term $\Delta\boldsymbol{T}$ is regular in both $\boldsymbol{r}_1$ and $\boldsymbol{r}_2$ throughout the fluid region.

The force density $\boldsymbol{F}(\boldsymbol{r})$ can be expressed in terms of the incident field $\boldsymbol{v}_0$ and the rigid body motion of the sphere through a grand resistance operator $\boldsymbol{Z}(\boldsymbol{r}_1,\boldsymbol{r}_2)$ [22],

$$\boldsymbol{F}(\boldsymbol{r}_1) = -\int \boldsymbol{Z}(\boldsymbol{r}_1,\boldsymbol{r}_2)\cdot[\boldsymbol{v}_0(\boldsymbol{r}_2) - \boldsymbol{u}(\boldsymbol{r}_2)]\,d\boldsymbol{r}_2\,. \tag{8}$$

Here the field $\boldsymbol{u}(\boldsymbol{r})$ describes the rigid body motion of the sphere,

$$\boldsymbol{u}(\boldsymbol{r}) = [\boldsymbol{U} + \boldsymbol{\Omega}\times(\boldsymbol{r}-\boldsymbol{R})]\,\theta(a - |\boldsymbol{r}-\boldsymbol{R}|)\,, \tag{9}$$

with a the particle radius, $\boldsymbol{R}$ the position of its centre, θ the Heaviside step function and $\boldsymbol{U}$, $\boldsymbol{\Omega}$ denoting respectively the rigid body translational and angular velocities of the particle.

3. Representations of the Green tensor

The Green tensor $\boldsymbol{T}(\boldsymbol{r}_1,\boldsymbol{r}_2)$ for a hard wall boundary is an explicit, but complicated, function of $\boldsymbol{r}_1$ and $\boldsymbol{r}_2$. It can be written in different forms using the Lorentz reflection theorem [6], or taking a limiting case of the Green tensor for a fluid–fluid interface [25,26], or expressing it in terms of a simple image system as did Blake [27]. Given a form for $\boldsymbol{T}$, the grand resistance operator can be calculated by expanding $\boldsymbol{v}, \boldsymbol{v}_0, \boldsymbol{T}$ in a basis set of functions with suitable spherical symmetry. For such a calculation we utilize two complete sets of solutions to the homogeneous Stokes equations (2) defined in Ref. [28]. These are denoted $\boldsymbol{v}^{+}_{lm\sigma}(\boldsymbol{r})$ and $\boldsymbol{v}^{-}_{lm\sigma}(\boldsymbol{r})$, where $\boldsymbol{v}^{+}_{lm\sigma}$ is regular at $\boldsymbol{r}=0$ and divergent at infinity while $\boldsymbol{v}^{-}_{lm\sigma}$ is singular at $\boldsymbol{r}=0$ and vanishes at infinity. This set is equivalent to that due to Lamb [29] but is expressed in terms of the vector spherical harmonics used commonly in electromagnetic theory or quantum mechanics [28]. The explicit definition of the functions $\boldsymbol{v}^{+}_{lm\sigma}$ is quoted in the Appendix to the present article. The labels $lm\sigma$ take the values $l=1,2,3,\ldots$, $m=-l,-l+1,\ldots,l-1,l$ and $\sigma=0,1,2$. This basis set enables us to expand the Oseen tensor $\boldsymbol{T}_0$ in a simple way about an arbitrary origin $\boldsymbol{r}_0$ [24],

$$\boldsymbol{T}_0(\boldsymbol{r}_1-\boldsymbol{r}_2)=\frac{1}{\eta}\sum_{lm\sigma}\frac{1}{n^2_{lm}}\boldsymbol{v}^{-}_{lm\sigma}(\boldsymbol{r}_>)\boldsymbol{v}^{+*}_{lm\sigma}(\boldsymbol{r}_<)\,, \tag{10}$$

where $\boldsymbol{r}_>$, $\boldsymbol{r}_<$ refer respectively to the larger and smaller of the relative position vectors $\boldsymbol{r}_1-\boldsymbol{r}_0$, $\boldsymbol{r}_2-\boldsymbol{r}_0$, and n_{lm} is a normalization constant

$$n_{lm}=\left[\frac{4\pi}{2l+1}\frac{(l+m)!}{(l-m)!}\right]^{1/2}. \tag{11}$$

We will now show that it is possible to write $\Delta\boldsymbol{T}$ in terms of the Oseen tensor $\boldsymbol{T}_0$ in such a way that we can use the expansion (10) to get a compact representation of the action of $\boldsymbol{T}$ on a given force density $\boldsymbol{F}$.

The geometry we consider is shown in Fig. 1 where the fluid occupies the half-space $z>0$ with $z=0$ corresponding to the hard wall. The unit vector $\hat{\boldsymbol{k}}$ is normal to the wall pointing into the fluid. We use the notation $\boldsymbol{r}_1$ for a field point where the flow $\boldsymbol{v}_1$ is to be determined and $\boldsymbol{r}_2$ for a source point where the force density $\boldsymbol{F}$ acts. We introduce the reflection operator $\boldsymbol{P}$

$$\boldsymbol{P}=\boldsymbol{1}-2\hat{\boldsymbol{k}}\,\hat{\boldsymbol{k}}\,, \tag{12}$$

which reflects a vector in the $z=0$ plane. If $\boldsymbol{r}_2=(x_2,y_2,z_2)$ is a source point, we use a prime to denote its image with respect to reflection in the wall, $\boldsymbol{r}'_2=\boldsymbol{P}\cdot\boldsymbol{r}_2=(x_2,y_2,-z_2)$.

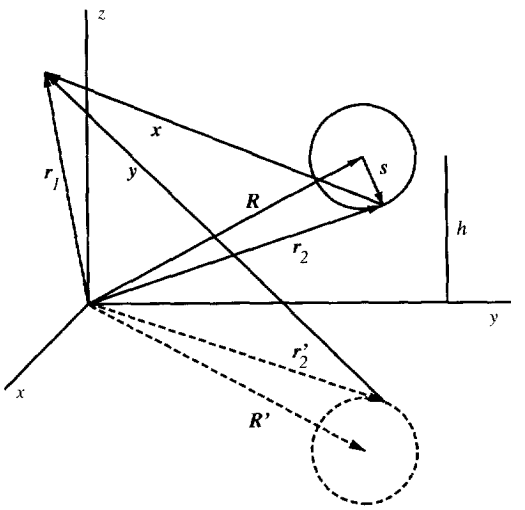


Fig. 1. Geometrical variables associated with the sphere and its image as used in Section 3. The hard wall corresponds to the plane $z = 0$.

The centre of the sphere at position $\boldsymbol{R} = (R_x, R_y, R_z)$ is at a height $h = R_z$ above the wall and the image sphere has its centre at $\boldsymbol{R}' = \boldsymbol{P} \cdot \boldsymbol{R}$.

If we first consider the part of the flow response to $\boldsymbol{F}(\boldsymbol{r})$ which is mediated by the contribution of the Oseen tensor in Eq. (6), then we can take an origin at the centre of the sphere $\boldsymbol{R}$ and use the expansion (10) to write

$$\boldsymbol{T}_0(\boldsymbol{r}_1 - \boldsymbol{r}_2) = \frac{1}{\eta} \sum_{lm\sigma} \frac{1}{n_{lm}^2} \boldsymbol{v}_{lm\sigma}^{-}(\boldsymbol{r}_1 - \boldsymbol{R}) \boldsymbol{v}_{lm\sigma}^{+*}(\boldsymbol{r}_2 - \boldsymbol{R}) , \tag{13}$$

giving a response

$$\int \boldsymbol{T}_0(\boldsymbol{r}_1 - \boldsymbol{r}_2) \cdot \boldsymbol{F}(\boldsymbol{r}_2)\, d\boldsymbol{r}_2 = \frac{1}{\eta} \sum_{lm\sigma} \frac{1}{n_{lm}^2} f_{lm\sigma} \boldsymbol{v}_{lm\sigma}^{-}(\boldsymbol{r}_1 - \boldsymbol{R}) . \tag{14}$$

Here we have introduced the spherical force multipoles exerted by the particle on the fluid which are defined by

$$f_{lm\sigma} = \int \boldsymbol{v}_{lm\sigma}^{+*}(\boldsymbol{r}_2 - \boldsymbol{R}) \cdot \boldsymbol{F}(\boldsymbol{r}_2)\, d\boldsymbol{r}_2 = \int \boldsymbol{v}_{lm\sigma}^{+*}(\boldsymbol{s}) \cdot \boldsymbol{F}(\boldsymbol{s})\, d\boldsymbol{s} , \tag{15}$$

where we write the integral finally in terms of the radial position vector with respect to the sphere centre, $\boldsymbol{s} = \boldsymbol{r}_2 - \boldsymbol{R}$ and $\boldsymbol{F}(\boldsymbol{s})$ denotes the force density as a function of this variable. We may write this in a compact scalar product notation as

$$f_{lm\sigma} = \langle \boldsymbol{v}_{lm\sigma}^{+} | \boldsymbol{F} \rangle \tag{16}$$

where the scalar product is defined as

$$\langle \boldsymbol{f} | \boldsymbol{g} \rangle = \int \boldsymbol{f}^*(\boldsymbol{r}) \cdot \boldsymbol{g}(\boldsymbol{r})\, d\boldsymbol{r} . \tag{17}$$

In an unbounded fluid, Eq. (14) would give the entire flow response directly as a superposition of independent contributions from each force multipole moment.

Next we wish to express the response mediated by the complete Green tensor $\boldsymbol{T}$ in terms of these multipoles as well. To do this we start from an expression for $\boldsymbol{T}$ due to Blake [27]. For a delta function force density, $\boldsymbol{F}(\boldsymbol{r}) = \boldsymbol{F}_0\delta(\boldsymbol{r} - \boldsymbol{r}_2)$, Blake gave the flow response in the presence of a wall as

$$\boldsymbol{v}_1(\boldsymbol{r}_1) = \boldsymbol{T}_0(\boldsymbol{x}) \cdot \boldsymbol{F}_0 - \boldsymbol{T}_0(\boldsymbol{y}) \cdot \boldsymbol{F}_0 - 2z_2\boldsymbol{F}_0 \cdot \boldsymbol{P} \cdot \nabla_y \boldsymbol{T}_0(\boldsymbol{y}) \cdot \hat{\boldsymbol{k}} + \frac{1}{8\pi\eta} 2z_2 \boldsymbol{F}_0 \cdot \boldsymbol{P} \cdot \nabla_y \left(\frac{z_2 \boldsymbol{y}}{y^3} \right), \tag{18}$$

where $\boldsymbol{x} = \boldsymbol{r}_1 - \boldsymbol{r}_2$ and $\boldsymbol{y} = \boldsymbol{r}_1 - \boldsymbol{r}_2'$ as defined in Fig. 1 and ∇_y is the gradient with respect to the variable $\boldsymbol{y}$. Use of the results (4) and (7) enables us to express the last part of $\boldsymbol{v}_1(\boldsymbol{r}_1)$ in terms of a Laplacian acting upon $\boldsymbol{T}_0(\boldsymbol{y})$. One can then show that the total response to a general force density can be expressed as

$$\begin{aligned} \boldsymbol{v}_1(\boldsymbol{r}_1) &= \int \boldsymbol{T}(\boldsymbol{r}_1, \boldsymbol{r}_2) \cdot \boldsymbol{F}(\boldsymbol{r}_2)\, d\boldsymbol{r}_2 \\ &= \int \boldsymbol{T}_0(\boldsymbol{r}_1 - \boldsymbol{r}_2) \cdot \boldsymbol{F}(\boldsymbol{r}_2)\, d\boldsymbol{r}_2 \\ &\quad - \int \boldsymbol{T}_0(\boldsymbol{r}_1 - \boldsymbol{r}_2') \cdot \boldsymbol{F}(\boldsymbol{P} \cdot \boldsymbol{r}_2')\, d\boldsymbol{r}_2' \\ &\quad - \int \boldsymbol{T}_0(\boldsymbol{r}_1 - \boldsymbol{r}_2') \cdot \hat{\boldsymbol{k}}\, \overleftarrow{\nabla}_{r_2'} \cdot \boldsymbol{P} \cdot \boldsymbol{F}(\boldsymbol{P} \cdot \boldsymbol{r}_2')\, 2z_2'\, d\boldsymbol{r}_2' \\ &\quad + \int \boldsymbol{T}_0(\boldsymbol{r}_1 - \boldsymbol{r}_2')\, \overleftarrow{\nabla}^2_{r_2'} \cdot \boldsymbol{P} \cdot \boldsymbol{F}(\boldsymbol{P} \cdot \boldsymbol{r}_2')\, z_2'^2\, d\boldsymbol{r}_2' \,. \end{aligned} \tag{19}$$

Note that the last three integrals have been expressed as integrations over the image sphere. The gradient and Laplacian operators, $\nabla_{r_2'}$ and $\nabla^2_{r_2'}$ are taken with respect to $\boldsymbol{r}_2'$ and the backward arrow above indicates that the derivatives act to the left on $\boldsymbol{T}_0(\boldsymbol{r}_1 - \boldsymbol{r}_2')$ rather than to the right. In each term we can introduce the expansion of $\boldsymbol{T}_0$ given in Eq. (10) using either the centre of the sphere $\boldsymbol{R}$ or that of the image sphere $\boldsymbol{R}'$ as the origin about which the expansion is taken. For the terms involving integration over the image sphere we can equivalently express them as integrations over the actual sphere in terms of the relative position variable $\boldsymbol{s} = \boldsymbol{r}_2 - \boldsymbol{R}$. By use of the identity (A.6) derived in Appendix A, $\boldsymbol{P} \cdot \boldsymbol{v}^+_{lm\sigma}(\boldsymbol{P} \cdot \boldsymbol{s}) = (-1)^{l+m+\sigma} \boldsymbol{v}^+_{lm\sigma}(\boldsymbol{s})$, we can reduce Eq. (19) to the form

$$\boldsymbol{v}_1(\boldsymbol{r}_1) = \frac{1}{\eta} \sum_{lm\sigma} \frac{1}{n^2_{lm}} [\boldsymbol{v}^-_{lm\sigma}(\boldsymbol{r}_1 - \boldsymbol{R}) - (-1)^{l+m+\sigma} \boldsymbol{v}^-_{lm\sigma}(\boldsymbol{r}_1 - \boldsymbol{R}')] \int \boldsymbol{v}^{+*}_{lm\sigma}(\boldsymbol{s}) \cdot \boldsymbol{F}(\boldsymbol{s})\, d\boldsymbol{s}$$

$$-\frac{1}{\eta}\sum_{lm\sigma}\frac{(-1)^{l+m+\sigma}}{n_{lm}^2}\boldsymbol{v}^-_{lm\sigma}(\boldsymbol{r}_1-\boldsymbol{R}')\int[-(h+s_z)^2\nabla_s^2\boldsymbol{v}^{+*}_{lm\sigma}(\boldsymbol{s})$$
$$+2(h+s_z)\boldsymbol{\nabla}_s(\hat{\boldsymbol{k}}\cdot\boldsymbol{v}^{+*}_{lm\sigma}(\boldsymbol{s}))-2\boldsymbol{v}^{+*}_{lm\sigma}(\boldsymbol{s})\cdot\hat{\boldsymbol{k}}\,\hat{\boldsymbol{k}}]\cdot\boldsymbol{F}(\boldsymbol{s})\,d\boldsymbol{s}\,. \tag{20}$$

The first part of the decomposition in Eq. (20) is expressed in terms of force multipoles. In the second part we can also obtain an expression in terms of force multipoles by use of the following identity discussed in Appendix A:

$$-(h+s_z)^2\nabla_s^2\boldsymbol{v}^+_{lm\sigma}(\boldsymbol{s})+2(h+s_z)\boldsymbol{\nabla}_s(\hat{\boldsymbol{k}}\cdot\boldsymbol{v}^+_{lm\sigma}(\boldsymbol{s}))-2\boldsymbol{v}^+_{lm\sigma}(\boldsymbol{s})\cdot\hat{\boldsymbol{k}}\,\hat{\boldsymbol{k}}$$
$$=\sum_{l_1m_1\sigma_1}\mathscr{C}(h;lm\sigma,l_1m_1\sigma_1)\boldsymbol{v}^+_{l_1m_1\sigma_1}(\boldsymbol{s})\,. \tag{21}$$

The matrix $\mathscr{C}(h;lm\sigma,l_1m_1\sigma_1)$ depends upon h and is diagonal in m, m_1 so that, for given $lm\sigma$, it has non-vanishing elements only for $l_1=l-2,l-1,l,l+1,l+2$ and $m=m_1$. By use of this identity in Eq. (20) we obtain the flow field $\boldsymbol{v}_1$ in the form

$$\boldsymbol{v}_1(\boldsymbol{r}_1)=\frac{1}{\eta}\sum_{lm\sigma}\frac{1}{n_{lm}^2}f_{lm\sigma}\boldsymbol{v}^-_{lm\sigma}(\boldsymbol{r}_1-\boldsymbol{R})+\frac{1}{\eta}\sum_{lm\sigma}\frac{1}{n_{lm}^2}f'_{lm\sigma}(h)\boldsymbol{v}^-_{lm\sigma}(\boldsymbol{r}_1-\boldsymbol{R}')\,, \tag{22}$$

where

$$f'_{lm\sigma}(h)=\sum_{l_1m_1\sigma_1}\mathscr{R}(h;lm\sigma,l_1m_1\sigma_1)f_{l_1m_1\sigma_1}\,, \tag{23}$$

with

$$\mathscr{R}(h;lm\sigma,l_1m_1\sigma_1)=(-1)^{l+m+\sigma+1}\delta_{mm_1}[\delta_{ll_1}\delta_{\sigma\sigma_1}+\mathscr{C}(h;lm\sigma,l_1m_1\sigma_1)]\,. \tag{24}$$

Thus the flow response to a spherical particle near a hard wall can be represented in terms of a superposition of a set of force multipoles $f_{lm\sigma}$ located on the sphere centred at $\boldsymbol{R}$ and a set of multipoles $f'_{lm\sigma}(h)$ located on the image sphere centred at $\boldsymbol{R}'$ with the $f'_{lm\sigma}(h)$ given as a linear combination of the $f_{lm\sigma}$. The matrix elements $\mathscr{R}(h;lm\sigma,l_1m_1\sigma_1)$ are tabulated in Appendix A.

We may express this result in terms of an expansion theorem for the exact Green tensor $\boldsymbol{T}$ for a hard wall analogous to the expansion of $\boldsymbol{T}_0$ given in Eq. (10),

$$\boldsymbol{T}(\boldsymbol{r}_1,\boldsymbol{r}_2)=\frac{1}{\eta}\sum_{lm\sigma}\frac{1}{n_{lm}^2}\boldsymbol{v}^-_{lm\sigma}(\boldsymbol{r}_>)\boldsymbol{v}^{+*}_{lm\sigma}(\boldsymbol{r}_<)$$
$$+\frac{1}{\eta}\sum_{lm\sigma;l_1m_1\sigma_1}\frac{1}{n_{lm}^2}\boldsymbol{v}^-_{lm\sigma}(\boldsymbol{r}'_>)\mathscr{R}(h;lm\sigma,l_1m_1\sigma_1)\boldsymbol{v}^{+*}_{l_1m_1\sigma_1}(\boldsymbol{r}_<)\,, \tag{25}$$

where, if $\boldsymbol{r}_0$ is an arbitrary point in the fluid above the wall, $\boldsymbol{r}_>$ and $\boldsymbol{r}_<$ have the same meaning as in Eq. (10) while $\boldsymbol{r}'_>$ denotes $\boldsymbol{r}_>$ with $\boldsymbol{r}_0$ replaced by its image $\boldsymbol{r}'_0$ with respect to the wall.

It is of interest to contrast this result with that for a planar boundary which is a free surface rather than a hard wall. With free surface boundary conditions at $z=0$ the Green tensor has the form [24]

$$\boldsymbol{T}_F(\boldsymbol{r}_1,\boldsymbol{r}_2')=\boldsymbol{T}_0(\boldsymbol{r}_1-\boldsymbol{r}_2)+\boldsymbol{T}_0(\boldsymbol{r}_1-\boldsymbol{r}_2')\cdot\boldsymbol{P}\,, \tag{26}$$

which leads to a simpler flow response

$$\boldsymbol{v}_{1F}(\boldsymbol{r}_1)=\frac{1}{\eta}\sum_{lm\sigma}\frac{1}{n_{lm}^2}f_{lm\sigma}[\boldsymbol{v}_{lm\sigma}^-(\boldsymbol{r}_1-\boldsymbol{R})+(-1)^{l+m+\sigma}\boldsymbol{v}_{lm\sigma}^-(\boldsymbol{r}_1-\boldsymbol{R}')]\,. \tag{27}$$

In this case the image multipoles are, apart from sign, identical with the original multipoles.

The collective properties of a suspension of spheres depend on the hydrodynamic interactions between spheres mediated by flow fields such as $\boldsymbol{v}_1$ and $\boldsymbol{v}_{1F}$. It is the long-ranged nature of these interactions which makes the study of suspension properties difficult. For bulk suspensions it is important in computer simulation studies to include all contributions to the flow field which fall off with distance no faster than $1/r^3$ [9]. The basis functions $\boldsymbol{v}_{lm\sigma}^-$ behave at large distance as $r^{-l-\sigma}$ so we see that in general many force multipoles must be taken into account. The presence of the boundary modifies the relative importance of different multipoles however. As an example, consider the lowest multipole f_{1m0} which gives the total force $\mathscr{F}$ exerted by the particle on the fluid,

$$f_{110}=-(\mathscr{F}_x+i\mathscr{F}_y),\quad f_{100}=\mathscr{F}_z,\quad f_{1-10}=\tfrac{1}{2}(\mathscr{F}_x-i\mathscr{F}_y)\,. \tag{28}$$

In unbounded fluid the flow arising from this net force dies out at large distance as $1/r$. Near a hard wall , however, the image multipoles modify this long distance behaviour. From the results (22)–(24), keeping the lowest multipole f_{1m0} and neglecting other multipoles, we find the flow response

$$\boldsymbol{v}_1(\boldsymbol{r}_1)\approx\frac{1}{\eta}\sum_{m}\frac{1}{n_{1m}^2}f_{1m0}[\boldsymbol{v}_{1m0}^-(\boldsymbol{r}_1-\boldsymbol{R})-\boldsymbol{v}_{1m0}^-(\boldsymbol{r}_1-\boldsymbol{R}')]\,. \tag{29}$$

As $r_1\to\infty$ the leading $1/r_1$ term due to the sphere is cancelled by its image so that the response dies away as $1/r_1^2$. We may contrast this with the free surface result,

$$\boldsymbol{v}_{1F}(\boldsymbol{r}_1)\approx\frac{1}{\eta}\sum_{m}\frac{1}{n_{1m}^2}f_{1m0}[\boldsymbol{v}_{1m0}^-(\boldsymbol{r}_1-\boldsymbol{R})-(-1)^m\boldsymbol{v}_{1m0}^-(\boldsymbol{r}_1-\boldsymbol{R}')]\,. \tag{30}$$

Here the response to $\mathscr{F}_z$ ($m=0$) falls off as $1/r_1^2$ while for the components of net force parallel to the free surface, $\mathscr{F}_x$, $\mathscr{F}_y$ ($m=\pm 1$), there is no cancellation and the long distance behaviour $1/r_1$ is enhanced relative to an unbounded fluid. The simplest computer simulation schemes [7,17] keep only the multipoles f_{1m0} (force), f_{1m1} (torque) and f_{2m0} (force dipole). However if we keep all the long distance fields (those vanishing no faster than $1/r_1^3$) we must investigate also the multipoles f_{3m0}, f_{2m1} and f_{1m2} [9].

4. Grand resistance operator

Because of the linearity of the Stokes flow equations, there is a linear relation between the moments of the force density $\boldsymbol{F}(\boldsymbol{r})$ and the derivatives of the driving field $\boldsymbol{v}_0(\boldsymbol{r}) - \boldsymbol{u}(\boldsymbol{r})$ evaluated at the centre of the sphere. This relation defines the friction matrix [28]

$$\begin{pmatrix} \mathscr{F} \\ \mathscr{T} \\ \mathscr{F}^{(2S)} \\ \vdots \end{pmatrix} = - \begin{pmatrix} \zeta^{tt} & \zeta^{tr} & \zeta^{td} & \cdots \\ \zeta^{rt} & \zeta^{rr} & \zeta^{rd} & \cdots \\ \zeta^{dt} & \zeta^{dr} & \zeta^{dd} & \cdots \\ \vdots & \vdots & \vdots & \ddots \end{pmatrix} \begin{pmatrix} \boldsymbol{v}_0(\boldsymbol{R}) - \boldsymbol{U} \\ \omega_0(\boldsymbol{R}) - \Omega \\ \boldsymbol{g}_0(\boldsymbol{R}) \\ \vdots \end{pmatrix}. \tag{31}$$

Here the net force, torque and symmetric force dipole moment exerted by the particle on the fluid are defined by

$$\mathscr{F} = \int \boldsymbol{F}(\boldsymbol{r})\, d\boldsymbol{r}, \qquad \mathscr{T} = \int (\boldsymbol{r} - \boldsymbol{R}) \times \boldsymbol{F}(\boldsymbol{r})\, d\boldsymbol{r}\,,$$

$$\mathscr{F}^{(2S)} = \int [(\boldsymbol{r} - \boldsymbol{R})\boldsymbol{F}(\boldsymbol{r})]_S\, d\boldsymbol{r}\,, \tag{32}$$

where $[(\boldsymbol{r} - \boldsymbol{R})\boldsymbol{F}(\boldsymbol{r})]_S$ denotes the symmetric and traceless part of the second rank tensor $[(\boldsymbol{r} - \boldsymbol{R})\boldsymbol{F}(\boldsymbol{r})]$. The fields $\omega_0(\boldsymbol{R})$ and $g_0(\boldsymbol{R})$ are defined by

$$\omega_0(\boldsymbol{R}) = \tfrac{1}{2}\nabla \times \boldsymbol{v}_0(\boldsymbol{r})|_{\boldsymbol{r}=\boldsymbol{R}}, \qquad g_0(\boldsymbol{R}) = [\nabla \boldsymbol{v}_0(\boldsymbol{r})]_S|_{\boldsymbol{r}=\boldsymbol{R}}\,. \tag{33}$$

As shown earlier [24], the friction tensors ζ can be calculated from matrix elements $Z(l_1 m_1 \sigma_1, l_2 m_2 \sigma_2)$ of the grand resistance operator $\boldsymbol{Z}$ taken with respect to the basis functions $\boldsymbol{v}^+_{lm\sigma}$,

$$Z(l_1 m_1 \sigma_1, l_2 m_2 \sigma_2) = \int \boldsymbol{v}^{+*}_{l_1 m_1 \sigma_1}(\boldsymbol{r}_1 - \boldsymbol{R}) \cdot \boldsymbol{Z}(\boldsymbol{r}_1, \boldsymbol{r}_2) \cdot \boldsymbol{v}^+_{l_2 m_2 \sigma_2}(\boldsymbol{r}_2 - \boldsymbol{R})\, d\boldsymbol{r}_1 d\boldsymbol{r}_2$$

$$= \langle \boldsymbol{v}^+_{l_1 m_1 \sigma_1}(1) | \boldsymbol{Z} | \boldsymbol{v}^+_{l_2 m_2 \sigma_2}(1) \rangle\,. \tag{34}$$

Here we introduce the notation $\boldsymbol{v}^{\pm}_{l_1 m_1 \sigma_1}(1)$ as shorthand for the functions $\boldsymbol{v}^{\pm}_{l_1 m_1 \sigma_1}(\boldsymbol{r} - \boldsymbol{R})$ which are centred at $\boldsymbol{R}$, the position of particle 1. The matrix $\boldsymbol{Z}$ is invertible and may be calculated from the matrix equation

$$\boldsymbol{Z}^{-1} = \boldsymbol{Z}_0^{-1} + \boldsymbol{D}\,, \tag{35}$$

where $\boldsymbol{Z}_0$ is the known grand resistance operator for unbounded fluid [28] and the matrix $\boldsymbol{D}$ is defined by the following expansion of $\Delta \boldsymbol{T}$,

$$\Delta \boldsymbol{T}(\boldsymbol{r}_1, \boldsymbol{r}_2) = \sum_{l_1 m_1 \sigma_1; l_2 m_2 \sigma_2} D(l_1 m_1 \sigma_1, l_2 m_2 \sigma_2) \boldsymbol{v}^+_{l_1 m_1 \sigma_1}(\boldsymbol{r}_1 - \boldsymbol{R}) \boldsymbol{v}^{+*}_{l_2 m_2 \sigma_2}(\boldsymbol{r}_2 - \boldsymbol{R})\,, \tag{36}$$

with

$$D(l_1 m_1 \sigma_1, l_2 m_2 \sigma_2) = \langle \boldsymbol{w}^+_{l_1 m_1 \sigma_1}(1) \delta_b(1) | \Delta \boldsymbol{T} | \boldsymbol{w}^+_{l_2 m_2 \sigma_2}(1) \delta_b(1) \rangle\,. \tag{37}$$

The functions $\boldsymbol{w}^{\pm}_{lm\sigma}(1)$ are an adjoint set of functions [28] centred on $\boldsymbol{R}$ and orthonormal to the functions $\boldsymbol{v}^{\pm}_{lm\sigma}(\boldsymbol{r})$ on the surface of a sphere of arbitrary radius b in the following sense:

$$\left\langle \boldsymbol{w}^{\pm}_{l_1m_1\sigma_1}(1)\delta_b(1)|\boldsymbol{v}^{\pm}_{l_2m_2\sigma_2}(1)\right\rangle = \int \boldsymbol{w}^{\pm *}_{l_1m_1\sigma_1}(\boldsymbol{r}-\boldsymbol{R})\frac{1}{b}\delta(|\boldsymbol{r}-\boldsymbol{R}|-b)\cdot \boldsymbol{v}^{\pm}_{l_2m_2\sigma_2}(\boldsymbol{r}-\boldsymbol{R})\,d\boldsymbol{r}$$

$$= \delta_{l_1l_2}\delta_{m_1m_2}\delta_{\sigma_1\sigma_2}\,. \tag{38}$$

We use $\delta_b(1)$ as shorthand for $\frac{1}{b}\delta(|\boldsymbol{r}-\boldsymbol{R}|-b)$ which is localized by the delta function to the spherical surface of radius b centred on $\boldsymbol{R}$. The earlier calculation of D for a hard wall [25] was cumbersome and lengthy but with the new representation of $\Delta\boldsymbol{T}$ can be carried out more easily.

In the matrix element (37) we have first to calculate $\Delta\boldsymbol{T}|\boldsymbol{w}^{+}_{l_2m_2\sigma_2}(1)\delta_b(1)\rangle$ which is just the velocity response propagated by $\Delta\boldsymbol{T}$ from a surface force density source $\boldsymbol{F}^{+}_{l_2m_2\sigma_2}(1)=\boldsymbol{w}^{+}_{l_2m_2\sigma_2}(1)\delta_b(1)$. This response follows from Eq. (22) as

$$\Delta\boldsymbol{T}|\boldsymbol{w}^{+}_{l_2m_2\sigma_2}(1)\delta_b(1)\rangle = \frac{1}{\eta}\sum_{lm\sigma}\frac{1}{n^2_{lm}}f'_{lm\sigma}(h)\boldsymbol{v}^{-}_{lm\sigma}(\boldsymbol{r}_1-\boldsymbol{R}')\,, \tag{39}$$

and the $f'_{lm\sigma}(h)$ are given by Eq. (23) in terms of the force multipoles

$$f_{l_1m_1\sigma_1} = \left\langle \boldsymbol{v}^{+}_{l_1m_1\sigma_1}(1)|\boldsymbol{F}^{+}_{l_2m_2\sigma_2}(1)\right\rangle = \delta_{l_1l_2}\delta_{m_1m_2}\delta_{\sigma_1\sigma_2}\,. \tag{40}$$

Thus the image multipoles $f'_{lm\sigma}(h)$ have the simple form

$$f'_{lm\sigma}(h) = \mathscr{R}(h; lm\sigma, l_2m_2\sigma_2) \tag{41}$$

leading to the result

$$D(l_1m_1\sigma_1, l_2m_2\sigma_2)$$

$$= \frac{1}{\eta}\sum_{lm\sigma}\frac{1}{n^2_{lm}}\left\langle \boldsymbol{w}^{+}_{l_1m_1\sigma_1}(1)\delta_b(1)|\boldsymbol{v}^{-}_{lm\sigma}(1')\right\rangle \mathscr{R}(h; lm\sigma, l_2m_2\sigma_2)\,, \tag{42}$$

where $\boldsymbol{v}^{-}_{lm\sigma}(1')$ is centred at the image point $\boldsymbol{R}'$. We can evaluate the first expression in Eq. (42), which involves the overlap of a function $\boldsymbol{w}^{+}$ centred at $\boldsymbol{R}$ with a function $\boldsymbol{v}^{-}$ centred at $\boldsymbol{R}'$, by use of the displacement theorems for the functions $\boldsymbol{v}^{\pm}_{lm\sigma}$ derived elsewhere [30]. In the notation of that reference we have

$$\left\langle \boldsymbol{w}^{+}_{l_1m_1\sigma_1}(1)\delta_b(1)|\boldsymbol{v}^{-}_{lm\sigma}(1')\right\rangle = S^{+-}(\boldsymbol{R}-\boldsymbol{R}'; l_1m_1\sigma_1, lm\sigma)\,, \tag{43}$$

giving a simple form for the matrix D,

$$D(l_1m_1\sigma_1, l_2m_2\sigma_2) = \frac{1}{\eta}\sum_{lm\sigma}\frac{1}{n^2_{lm}}S^{+-}(\boldsymbol{R}-\boldsymbol{R}'; l_1m_1\sigma_1, lm\sigma)\mathscr{R}(h; lm\sigma, l_2m_2\sigma_2)\,. \tag{44}$$

The function S^{+-} is given explicitly in Ref. [30] and from the definition of the matrix $\mathscr{R}$ it follows that the summation in Eq. (44) is a finite sum only. Since

$\boldsymbol{R}-\boldsymbol{R}'=2h\hat{\boldsymbol{k}}$, S^{--} is diagonal in m_1, m [30] and $\mathscr{R}$, from Eq. (24), is diagonal in m, m_2 so that D is itself diagonal in m_1, m_2. For free surface boundary conditions we again get a simplification compared with the earlier derivation [24]. We find for a free surface,

$$D_F(l_1m_1\sigma_1, l_2m_2\sigma_2)=\frac{(-1)^{l_2+m_2+\sigma_2}}{\eta n^2_{l_2m_2}}S^{+-}(\boldsymbol{R}-\boldsymbol{R}'; l_1m_1\sigma_1, l_2m_2\sigma_2)\,. \tag{45}$$

The results (44) and (45) greatly simplify the calculation of the matrix elements $Z(l_1m_1\sigma_1, l_2m_2\sigma_2)$ which may be obtained from Eqs. (35) and (44) as expansions in powers of a/h as explained elsewhere [24].

5. Scalar friction functions

The friction tensors defined in Eq. (31) can be expressed in terms of scalar friction functions together with irreducible tensors formed from the unit tensor, the Levi–Civita tensor and the vector $\hat{\boldsymbol{k}}$ normal to the bounding wall. The scalar functions depend on the ratio $t=a/h$ of particle radius a to distance h of its centre from the wall. To describe the motion of a sphere near a wall in a linear shear flow we need the tt, tr, rr, td and rd friction tensors. These have the decomposition

$$\begin{aligned}
\zeta^{\mathrm{tt}}_{\alpha\mu} &= \phi^{\mathrm{tt}}k_\alpha k_\mu + \psi^{\mathrm{tt}}(\delta_{\alpha\mu}-k_\alpha k_\mu)\,,\\
\zeta^{\mathrm{tr}}_{\alpha\mu} &= \psi^{\mathrm{tr}}\varepsilon_{\alpha\mu\sigma}k_\sigma\,,\\
\zeta^{\mathrm{td}}_{\alpha\mu\nu} &= \phi^{\mathrm{td}}k_\alpha\overbrace{k_\mu k_\nu}^{(\mu\nu)} + \psi^{\mathrm{td}}\overbrace{(\delta_{\alpha\mu}-k_\alpha k_\mu)k_\nu}^{(\mu\nu)}\,,\\
\zeta^{\mathrm{rt}}_{\alpha\mu} &= \psi^{\mathrm{rt}}\varepsilon_{\alpha\mu\sigma}k_\sigma\,,\\
\zeta^{\mathrm{rr}}_{\alpha\mu} &= \phi^{\mathrm{rr}}k_\alpha k_\mu + \psi^{\mathrm{rr}}(\delta_{\alpha\mu}-k_\alpha k_\mu)\,,\\
\zeta^{\mathrm{rd}}_{\alpha\mu\nu} &= \psi^{\mathrm{rd}}k_\sigma\overbrace{\varepsilon_{\sigma\alpha\mu}k_\nu}^{(\mu\nu)}\,,\\
\zeta^{\mathrm{dt}}_{\alpha\beta\mu} &= \phi^{\mathrm{dt}}\overbrace{k_\alpha k_\beta}^{(\alpha\beta)}k_\mu + \psi^{\mathrm{dt}}\overbrace{k_\alpha(\delta_{\beta\mu}-k_\beta k_\mu)}^{(\alpha\beta)}\,,\\
\zeta^{\mathrm{dr}}_{\alpha\beta\mu} &= \psi^{\mathrm{dr}}\overbrace{k_\alpha\varepsilon_{\beta\mu\sigma}}^{(\alpha\beta)}k_\sigma\,,
\end{aligned} \tag{46}$$

where the overbrace $\overbrace{}^{(\mu\nu)}$ denotes the symmetric and traceless part of the tensor expression with respect to the two tensor indices $\mu\nu$ and the summation convention applies. For example, a second rank tensor $T_{\mu\nu}$ has a symmetric and traceless part defined by

$$\overbrace{T_{\mu\nu}}^{(\mu\nu)} = \tfrac{1}{2}(T_{\mu\nu}+T_{\nu\mu})-\tfrac{1}{3}\delta_{\mu\nu}T_{\alpha\alpha}\,. \tag{47}$$

It follows from the Lorentz reciprocity theorem [28,23] that the grand resistance operator is symmetric and, hence, that the following symmetry relations hold for the friction tensors,

$$\zeta^{\mathrm{tr}}_{\alpha\mu} = \zeta^{\mathrm{rt}}_{\mu\alpha}, \qquad \zeta^{\mathrm{td}}_{\alpha\mu\nu} = \zeta^{\mathrm{dt}}_{\mu\nu\alpha}, \qquad \zeta^{\mathrm{rd}}_{\alpha\mu\nu} = \zeta^{\mathrm{dr}}_{\mu\nu\alpha}. \tag{48}$$

In terms of the scalar functions these relations become

$$\psi^{\mathrm{tr}} = -\psi^{\mathrm{rt}}, \qquad \phi^{\mathrm{td}} = \phi^{\mathrm{dt}}, \qquad \psi^{\mathrm{td}} = \psi^{\mathrm{dt}}, \qquad \psi^{\mathrm{rd}} = -\psi^{\mathrm{dr}}. \tag{49}$$

The scalar friction functions can be expressed as the following matrix elements of the grand resistance operator [24,25],

$$\begin{aligned}
&\phi^{\mathrm{tt}} = Z(100,100), && \psi^{\mathrm{tt}} = \tfrac{1}{2}Z(110,110),\\
&\phi^{\mathrm{rr}} = Z(101,101), && \psi^{\mathrm{rr}} = \tfrac{1}{2}Z(111,111),\\
&\phi^{\mathrm{dt}} = \tfrac{1}{2}Z(200,100), && \psi^{\mathrm{dt}} = \tfrac{1}{6}Z(210,110),\\
&\psi^{\mathrm{tr}} = -\tfrac{1}{2}Z(110,111), && \psi^{\mathrm{dr}} = -\tfrac{1}{6}Z(110,110).
\end{aligned} \tag{50}$$

Following the procedures outlined in Section 4 we can calculate each of these as a series of reflections in increasing powers of the variable t.

The series expressions converge rapidly for particles far from the wall, but at touching, for hard sphere particles with stick boundary conditions, all functions except ϕ^{rr} diverge. Henceforth we will consider only such hard sphere particles. For particles close to the wall the series convergence is quite slow so an accurate representation requires either hundreds of terms in the reflection series or else an asymptotic representation of the functions at near-touching distances. This latter regime, the lubrication regime, has been studied previously in a number of articles using numerical or analytical methods [31–36]. However, Jeffrey and Onishi [37] have independently studied the lubrication regime for the close approach of two unequal sized hard spheres. By taking the radius of one of these spheres to infinity it is possible to derive the asymptotic lubrication theory representation for the sphere-wall functions. To express these results it is convenient to introduce dimensionless friction functions defined as follows:

$$\begin{aligned}
\tilde{\phi}^{\mathrm{tt}} &= \phi^{\mathrm{tt}}/6\pi\eta a, && \tilde{\psi}^{\mathrm{tt}} = \psi^{\mathrm{tt}}/6\pi\eta a,\\
\tilde{\phi}^{\mathrm{rr}} &= \phi^{\mathrm{rr}}/8\pi\eta a^3, && \tilde{\psi}^{\mathrm{rr}} = \psi^{\mathrm{rr}}/8\pi\eta a^3,\\
\tilde{\phi}^{\mathrm{dt}} &= \phi^{\mathrm{dt}}/6\pi\eta a^2, && \tilde{\psi}^{\mathrm{dt}} = \psi^{\mathrm{dt}}/6\pi\eta a^2,\\
\tilde{\psi}^{\mathrm{tr}} &= \psi^{\mathrm{tr}}/8\pi\eta a^2, && \tilde{\psi}^{\mathrm{dr}} = \psi^{\mathrm{dr}}/8\pi\eta a^3.
\end{aligned} \tag{51}$$

As the sphere approaches the wall, $t \to 1$, the generic form of the asymptotic expansion of these functions is

$$\tilde{\phi} \approx C_1 \frac{t}{1-t} + C_2 \ln(1-t) + C_3 + C_4 \left(\frac{1-t}{t}\right) \ln(1-t) + \mathcal{O}(1-t), \tag{52}$$

where $\tilde{\phi}$ stands for any of the functions in Eq. (51). For two unequal spheres Jeffrey and Onishi [37] give exact expressions for the coefficients of the two-sphere asymptotic

series which, in the limit that one sphere becomes infinitely large, lead to exact values for C_1, C_2, C_4. We obtain approximate values for the constant C_3 (apart from the case of $\tilde{\phi}^{rr}$) from careful analysis of the reflection series to high order. We find the following asymptotic results:

$$\tilde{\phi}^{tt} = \frac{t}{1-t} - \frac{1}{5}\ln(1-t) + 0.97127 - \frac{1}{21}\left(\frac{1-t}{t}\right)\ln(1-t) + \cdots,$$

$$\tilde{\psi}^{tt} = -\frac{8}{15}\ln(1-t) + 0.95429 - \frac{64}{375}\left(\frac{1-t}{t}\right)\ln(1-t) + \cdots,$$

$$\tilde{\phi}^{rr} = \zeta(3) + \frac{1}{2}\left(\frac{1-t}{t}\right)\ln(1-t) + \cdots,$$

$$\tilde{\psi}^{rr} = -\frac{2}{5}\ln(1-t) + 0.37089 - \frac{66}{125}\left(\frac{1-t}{t}\right)\ln(1-t) + \cdots,$$

$$\tilde{\psi}^{tr} = \frac{1}{10}\ln(1-t) + 0.19295 + \frac{43}{250}\left(\frac{1-t}{t}\right)\ln(1-t) + \cdots,$$

$$\tilde{\phi}^{dt} = -\frac{t}{1-t} - \frac{4}{5}\ln(1-t) - 0.30697 - \frac{13}{21}\left(\frac{1-t}{t}\right)\ln(1-t) + \cdots,$$

$$\tilde{\psi}^{dt} = \frac{14}{15}\ln(1-t) + 1.23538 + \frac{442}{375}\left(\frac{1-t}{t}\right)\ln(1-t) + \cdots,$$

$$\tilde{\psi}^{dr} = \frac{1}{5}\ln(1-t) + 0.18719 - \frac{2}{125}\left(\frac{1-t}{t}\right)\ln(1-t) + \cdots, \tag{53}$$

where $\zeta(3)$ is the zeta function.

We have calculated the coefficients of the reflection series expansions of the friction functions through order t^{300}. By careful analysis of these series we have verified the values of the coefficients C_1, C_2, C_4 in the expressions above and have obtained the constant terms C_3 by extrapolation. To illustrate the technique we consider the case of $\tilde{\phi}^{dt}$ which has a series expansion

$$\tilde{\phi}(t) = \sum_{n=0}^{\infty} f_n t^n, \tag{54}$$

where we have dropped the explicit superscript dt for simplicity. We expect this series to diverge at $t=1$ corresponding to the physical phenomenon of the sphere touching the wall. However, the convergence of such a series may be affected by unphysical singularities of the function $\tilde{\phi}(t)$ at other values of t in the complex t-plane. This phenomenon is known to occur in the case of the reflection series for two equal spheres where symmetry leads to the friction functions being either even or odd functions of t with unphysical singularities at $t=-1$. In the present geometry there is no symmetry between sphere and plane but unphysical singularities may still limit the rate of convergence. In fact, we find evidence for a singularity structure at $t=-1$ as well as at $t=1$.

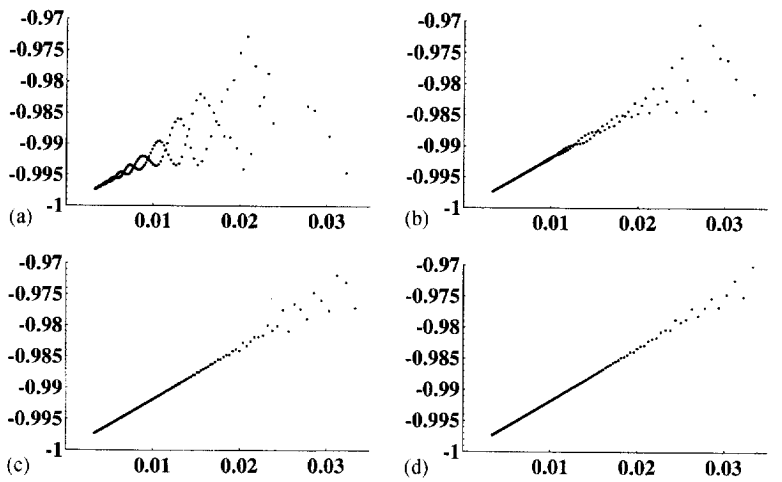


Fig. 2. In (a) the reflection series coefficients f_n (vertical axis) for $\tilde{\phi}^{\mathrm{dt}}$ are plotted against $1/n$ (horizontal axis) to show the oscillatory convergence as $n \to \infty$. In (b)–(d) we show improved convergence as explained after Eq. (56) by plots of $f_n^{(p)}$ against $1/n$ for $p = 1, 2, 3$, respectively.

For example, from the leading term in the asymptotic form of $\tilde{\phi}^{\mathrm{dt}}$ given in Eq. (53) we expect that $f_n \to -1$ in the limit $n \to \infty$. This is indeed so as shown in Fig. 2a where we plot f_n against $1/n$ but the convergence is oscillatory in nature. This oscillatory phenomenon is common to the series expansions for all the functions in Eq. (53). We find that this oscillatory behaviour can be controlled by introducing the associated functions $\tilde{\phi}^{(p)}$ defined by

$$\tilde{\phi}^{(0)}(t) = \tilde{\phi}(t), \qquad \tilde{\phi}^{(p)}(t) = \frac{1+t}{2}\tilde{\phi}^{(p-1)}(t), \tag{55}$$

with the series expansions

$$\tilde{\phi}^{(p)}(t) = \sum_{n=0}^{\infty} f_n^{(p)} t^n . \tag{56}$$

We expect that $f_n^{(p)} \to -1$ as $n \to \infty$ but the oscillations are damped by taking successively higher values of p. In Fig. 2b–2d we plot $f_n^{(p)}$ against $1/n$ for $p = 1, 2, 3$ respectively. No further improvement in convergence occurs in this case for higher values of p. The factors of $(1 + t)$ introduced in Eq. (55) damp out any singular structure in $\tilde{\phi}(t)$ at $t = -1$ and this is correlated with better convergence.

Knowing the leading terms in the asymptotic expressions (53) enables us to successively verify the exact numerical coefficients from the series data. Using $\tilde{\phi}^{\mathrm{dt}}$ as an example, we can subtract out the first two asymptotic contributions to get a residual series

$$\tilde{\phi}_r = \tilde{\phi} + \frac{t}{1-t} + \frac{4}{5}\ln(1-t) = f_0 + \sum_{n=1}^{\infty}\left(f_n + 1 - \frac{4}{5n}\right)t^n = \sum_{n=0}^{\infty} f_{rn} t^n . \tag{57}$$

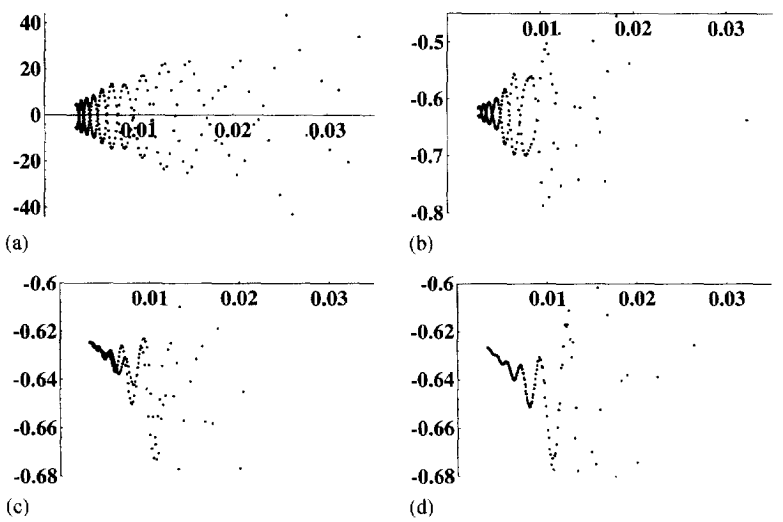


Fig. 3. Here we estimate the value of C_4 for $\tilde{\phi}^{\mathrm{dt}}$ by analysis of the residual series defined in Eq. (57). In (a) we plot $n^2 f_{rn}$ (vertical axis) against $1/n$ (horizontal axis). To get improved convergence as explained after Eq. (58), we plot $n^2 f_{rn}^{(p)}$ against $1/n$ for $p=2,3,4$ in (b)–(d), respectively.

We expect then that $n^2 f_{rn} \to -13/21$ as $n \to \infty$. In Fig. 3a we plot $n^2 f_{rn}$ against $1/n$, but the oscillations in the data make the limiting value impossible to discern. However, if we apply the same technique as above defining

$$\tilde{\phi}_r^{(p)}(t) = \frac{1+t}{2}\,\tilde{\phi}_r^{(p-1)}(t) = \sum_{n=0}^{\infty} f_{rn}^{(p)} t^n\,, \tag{58}$$

then the convergence becomes much clearer as shown in Fig. 3b–3d where we plot $n^2 f_{rn}^{(p)}$ against $1/n$ for $p=2,3,4$. The limiting value is seen to be consistent with $-13/21 \approx -0.619$.

To obtain the constant term (C_3) in the asymptotic representations we subtract out the first three exactly known asymptotic terms,

$$\begin{aligned}\tilde{\phi}_c(t) &= \tilde{\phi} + \frac{t}{1-t} + \frac{4}{5}\ln(1-t) + \frac{13}{21}\left(\frac{1-t}{t}\right)\ln(1-t) \\ &= f_0 - \frac{13}{21} + \sum_{n=1}^{\infty}\left(f_n + 1 - \frac{4}{5n} + \frac{13}{21n(n+1)}\right) t^n = \sum_{n=0}^{\infty} f_{cn} t^n\,. \end{aligned} \tag{59}$$

This function is finite at $t=1$ with a value equal to the constant C_3 which we seek. To obtain $\tilde{\phi}_c(1)$ we use a slightly different extrapolation method. Define

$$\tilde{\phi}_c^N(t) = \sum_{n=0}^{N} f_{cn} t^n\,. \tag{60}$$

By plotting $\tilde{\phi}_c^N(1)$ against $1/N$ we can extrapolate to $N \to \infty$ to obtain an estimate for $\tilde{\phi}_c(1)$. Fig. 4a illustrates this procedure. To control the oscillations we define

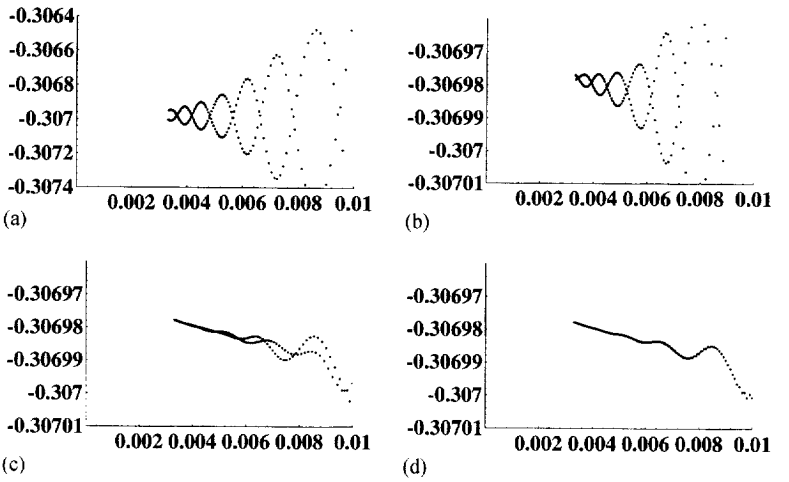


Fig. 4. Here we estimate the constant C_3 for $\tilde{\phi}^{\mathrm{dt}}$ by the method explained after Eqs. (60) and (61). In (a) we plot $\tilde{\phi}_c^N(1)$ (vertical axis) against $1/N$ (horizontal axis). In (b)–(d) we improve the convergence by plotting $\tilde{\phi}_c^{(p)N}(1)$ against $1/N$ for $p=1,2,3$, respectively.

successively as previously

$$\tilde{\phi}_c^{(p)}(t)=\frac{1+t}{2}\,\tilde{\phi}_c^{(p-1)}(t)=\sum_{n=0}^{\infty} f_{cn}^{(p)} t^n\,, \tag{61}$$

noting that $\tilde{\phi}_c^{(p)}(1)=\tilde{\phi}_c^{(p-1)}(1)$. Now, for each value of p, we truncate the series for $\tilde{\phi}_c^{(p)}(t)$ at the Nth term and set $t=1$. By plotting this value, $\tilde{\phi}_c^{(p)N}(1)$, against $1/N$ the rapid oscillations are removed leaving an easy extrapolation to determine $\tilde{\phi}_c(1)=\tilde{\phi}_c^{(p)}(1)$. Fig. 4b–4d illustrate this for $p=1,2,3$.

The asymptotic expressions given in Eq. (52) are accurate only in the regime of near touching, say $0.999<t<1$. For the range $0<t<0.5$ the series expansions may be truncated at order t^{20} to give highly accurate results. However, in the range $0.5<t<0.999$ one requires several hundred terms in the reflection series to get accurate values for the scalar friction functions. We have found a more succinct way to represent the friction functions accurately over the entire range $0\leqslant t\leqslant 1$. To explain this method we consider a typical friction function $\tilde{\phi}(t)$ with a reflection series as in Eq. (54) and an asymptotic behaviour at close approach as in Eq. (52). We subtract out of the reflection series the exactly known contributions of the asymptotic terms to get a more rapidly convergent remainder series [38],

$$\begin{aligned}\tilde{\phi}(t)-C_1\frac{t}{1-t}-C_2\ln(1-t)-C_4\left(\frac{1-t}{t}\right)\ln(1-t)\\ =f_0+C_4+\sum_{n=1}^{\infty}\left(f_n-C_1+\frac{C_2}{n}-\frac{C_4}{n(n+1)}\right)t^n=\sum_{n=0}^{\infty} g_n t^n\,.\end{aligned} \tag{62}$$

In the limit $n \to \infty$ we have $g_n \approx \mathcal{O}(1/n^3)$ so the remainder series converges faster than does the full reflection series but the convergence is still slow with the oscillatory patterns seen above. We have found that the series with coefficients g_n which are known up to $n = 300$ can be well represented in the range $0 \leqslant t \leqslant 1$ by a diagonal Padé approximant [39] involving many fewer constants. Thus we represent $\tilde{\phi}(t)$ for all physical t values $(0 \leqslant t \leqslant 1)$ as

$$\tilde{\phi}(t) = C_1 \frac{t}{1-t} + C_2 \ln(1-t) + C_4 \left(\frac{1-t}{t}\right) \ln(1-t) + \mathscr{P}_N(t), \tag{63}$$

where

$$\mathscr{P}_N(t) = \frac{a_0 + a_1 t + a_2 t^2 + \cdots + a_N t^N}{1 + b_1 t + b_2 t^2 + \cdots + b_N t^N}. \tag{64}$$

The coefficients a_i, b_i are fixed by demanding that the series expansion of $\mathscr{P}_N(t)$ about $t = 0$ should agree exactly with the remainder series to order t^{2N}. This requirement determines a_i, b_i as the solutions to the linear equations [39]

$$\begin{pmatrix} g_1 & g_2 & \cdots & g_N \\ g_2 & g_3 & \cdots & g_{N+1} \\ \vdots & \vdots & \vdots & \vdots \\ g_N & g_{N+1} & \cdots & g_{2N-1} \end{pmatrix} \begin{pmatrix} b_N \\ b_{N-1} \\ \vdots \\ b_1 \end{pmatrix} = - \begin{pmatrix} g_{N+1} \\ g_{N+2} \\ \vdots \\ g_{2N} \end{pmatrix}, \tag{65}$$

and

$$\begin{aligned} a_0 &= g_0, \\ a_i &= g_i + b_1 g_{i-1} + b_2 g_{i-2} + \cdots + b_i g_0, \quad i = 1, \ldots, N. \end{aligned} \tag{66}$$

We find that the remainder series for all the friction functions in Eq. (53) can be represented to an accuracy of better than 1 part in 2000 for all physical values of t by Padé approximants with $N \leqslant 16$. Thus instead of using 301 coefficients g_n we need only $2N + 1$ Padé coefficients. To construct the representation given in Eq. (63) we need then only the coefficients $f_0, \ldots, f_{2N}$ calculated by the procedure in Section 4, from which we calculate the coefficients $g_0, \ldots, g_{2N}$ as in (62) and obtain finally the a_i, b_i from Eqs. (65) and (66). Numerical studies show that for $\tilde{\phi}^{\mathrm{tt}}$ we need the Padé approximant of order $N = 7$, for $\tilde{\psi}^{\mathrm{tt}}$ we need $N = 6$, for $\tilde{\phi}^{\mathrm{rr}}$, $N = 8$, for $\tilde{\psi}^{\mathrm{rr}}$, $N = 9$, for $\tilde{\psi}^{\mathrm{tr}}$, $N = 9$, for $\tilde{\phi}^{\mathrm{dt}}$, $N = 14$, for $\tilde{\psi}^{\mathrm{dt}}$, $N = 10$, and for $\tilde{\psi}^{\mathrm{dr}}$, $N = 16$. We have already published [25] the expansion coefficients f_n for $n = 0, \ldots, 20$ for the functions $\tilde{\phi}^{\mathrm{tt}}$, $\tilde{\psi}^{\mathrm{tt}}$, $\tilde{\phi}^{\mathrm{rr}}$, $\tilde{\psi}^{\mathrm{rr}}$ and $\tilde{\psi}^{\mathrm{tr}}$. For the functions $\tilde{\phi}^{\mathrm{dt}}$, $\tilde{\psi}^{\mathrm{dt}}$ and $\tilde{\psi}^{\mathrm{dr}}$ we give the coefficients f_n for $n = 0, \ldots, 32$ in Tables 1 and 2. This information is sufficient to construct the approximate expressions (63) for all the above friction functions. Anyone who wishes to have the coefficients of the full reflection series to order t^{300} should contact one of the authors.

In an earlier study [25] the values of the friction functions $\tilde{\psi}^{\mathrm{tt}}$, $\tilde{\psi}^{\mathrm{tr}}$, $\tilde{\psi}^{\mathrm{rr}}$ as computed from reflection series to order t^{50} were shown to compare well with numerical values

Table 1
Numerical coefficients f_n of the terms t^n, $n=0,1,\ldots,32$ in the series expansion of the friction functions $\tilde{\phi}^{\mathrm{dt}}$ and $\tilde{\psi}^{\mathrm{dt}}$

n	$\tilde{\phi}^{\mathrm{dt}}$	$\tilde{\psi}^{\mathrm{dt}}$
0	0.0	0.0
1	0.0	0.0
2	−0.9375	−0.625
3	−1.0546875	−0.3515625
4	−0.2490234375	0.30224609375
5	−0.983276367188	−0.337799072266
6	−1.38572692871	−0.464263280233
7	−0.423231124878	0.276480078697
8	−0.978244543076	−0.235118307173
9	−1.12767860293	−0.182981772814
10	−0.531301852316	0.205336121697
11	−1.25671236543	−0.353879914973
12	−0.946503999585	−0.0369421793099
13	−0.715512079587	0.0738728256011
14	−1.1949880051	−0.229465155013
15	−0.796062326786	0.0417795128112
16	−0.937424471661	−0.03299250071
17	−1.04918259262	−0.114245227246
18	−0.888576668624	−0.0254647088538
19	−0.967221551738	−0.01171705143
20	−0.998240362428	−0.102684936893
21	−0.947860755895	−0.0231561980201
22	−0.927998071458	0.00150126887991
23	−1.0449581776	−0.118279223165
24	−0.889956433344	0.0337844199426
25	−1.00103343343	−0.0608090719165
26	−0.989175560413	−0.0500913290039
27	−0.917092783901	0.00146011012206
28	−1.02847405786	−0.0579169512443
29	−0.934576282876	−0.0202701008668
30	−0.994614775352	−0.0356258915975
31	−0.963527306651	−0.0161273953913
32	−0.988724203563	−0.052363261754

calculated by Goldman, Cox and Brenner [35]. In their second paper [36] they considered the effect of a shear flow and computed a force and torque denoted there by F_x^{S*} and T_y^{S*}, respectively. In the notation used above we can express these quantities as

$$F_x^{S*} = \tilde{\psi}^{\mathrm{tt}}(t) + \tfrac{2}{3}t\tilde{\psi}^{\mathrm{tr}}(t) + \tfrac{1}{2}t\tilde{\psi}^{\mathrm{dt}}, \qquad T_y^{S*} = \frac{2}{t}\tilde{\psi}^{\mathrm{tr}}(t) + \tilde{\psi}^{\mathrm{rr}}(t) + \tilde{\psi}^{\mathrm{dr}}(t). \tag{67}$$

These expressions thus involve the coupling of translations and rotations to the shear field. In Table 3 we compare the numerical values for these quantities as calculated by Goldman, Cox and Brenner [36] with the values given by the Padé approximations defined above. The numerical agreement is excellent.

Table 2
Numerical coefficients f_n of the terms t^n, $n=0,1,\ldots,32$ in the series expansion of the friction function $\tilde{\psi}^{\mathrm{dr}}$

n	$\tilde{\psi}^{\mathrm{dr}}$
0	0.0
1	0.0
2	0.0
3	−0.3125
4	0.0
5	0.25
6	−0.33203125
7	−0.02197265625
8	0.209320068359
9	−0.28814125061
10	0.0968316793442
11	0.0971943363547
12	−0.248299906496
13	0.1424751413
14	−0.0221396419893
15	−0.118279751836
16	0.103470684
17	−0.053445903987
18	−0.0396951782525
19	0.0321315731927
20	−0.0142718268152
21	−0.0507405013827
22	0.039072236415
23	−0.0232594354164
24	−0.0407837450168
25	0.0488662763077
26	−0.0539157740793
27	0.00864326982767
28	0.0033318764473
29	−0.0242871215042
30	0.00262653887094
31	−0.00630123364661
32	−0.00646882190348

6. Calculation of mobility functions

The linear relation (31) which defines the friction matrix may be partially inverted to define the mobility matrix [28]

$$\begin{pmatrix} \boldsymbol{v}_0(\boldsymbol{R})-\boldsymbol{U} \\ \boldsymbol{\omega}_0(\boldsymbol{R})-\boldsymbol{\Omega} \\ \mathscr{F}^{(2S)} \\ \vdots \end{pmatrix} = -\begin{pmatrix} \boldsymbol{\mu}^{\mathrm{tt}} & \boldsymbol{\mu}^{\mathrm{tr}} & \boldsymbol{\mu}^{\mathrm{td}} & \cdots \\ \boldsymbol{\mu}^{\mathrm{rt}} & \boldsymbol{\mu}^{\mathrm{rr}} & \boldsymbol{\mu}^{\mathrm{rd}} & \cdots \\ \boldsymbol{\mu}^{\mathrm{dt}} & \boldsymbol{\mu}^{\mathrm{dr}} & \boldsymbol{\mu}^{\mathrm{dd}} & \cdots \\ \vdots & \vdots & \vdots & \ddots \end{pmatrix} \begin{pmatrix} \mathscr{F} \\ \mathscr{T} \\ g_0(\boldsymbol{R}) \\ \vdots \end{pmatrix}, \tag{68}$$

Table 3
Numerical values from Goldman, Cox and Brenner [36] for the quantities in Eq. (67) compared with values calculated from the Padé approximation described in Section 5

$1/t$	F_x^{S*}		T_y^{S*}	
	Ref. [36]	Padé	Ref. [36]	Padé
10.0677	1.0587	1.0587	0.99981	0.99983
3.7622	1.1671	1.1671	0.99711	0.99710
2.3524	1.2780	1.2780	0.99010	0.99012
1.5431	1.4391	1.4391	0.97419	0.97423
1.1276	1.6160	1.6160	0.95374	0.95374
1.0453	1.6682	1.6684	0.94769	0.94768
1.005004	1.6969	1.6975	0.94442	0.94427
1.003202	1.6982	1.6989	0.94427	0.94410

and the mobility tensors $\boldsymbol{\mu}$. Note that only within the t-r sector do we have the simple inverse relation

$$\begin{pmatrix} \boldsymbol{\mu}^{\mathrm{tt}} & \boldsymbol{\mu}^{\mathrm{tr}} \\ \boldsymbol{\mu}^{\mathrm{rt}} & \boldsymbol{\mu}^{\mathrm{rr}} \end{pmatrix} = \begin{pmatrix} \boldsymbol{\zeta}^{\mathrm{tt}} & \boldsymbol{\zeta}^{\mathrm{tr}} \\ \boldsymbol{\zeta}^{\mathrm{rt}} & \boldsymbol{\zeta}^{\mathrm{rr}} \end{pmatrix}^{-1} . \tag{69}$$

From the requirement that Eqs. (31) and (68) be consistent we find the following symmetry properties of the mobility tensors:

$$\mu^{\mathrm{tr}}_{\alpha\mu} = \mu^{\mathrm{rt}}_{\mu\alpha} , \qquad \mu^{\mathrm{td}}_{\alpha\mu\nu} = -\mu^{\mathrm{dt}}_{\mu\nu\alpha} , \qquad \mu^{\mathrm{rd}}_{\alpha\mu\nu} = -\mu^{\mathrm{dr}}_{\mu\nu\alpha} . \tag{70}$$

These tensors have the same decomposition as do the friction tensors given in (46) with the scalar friction functions $\phi(t)$, $\psi(t)$ replaced by scalar mobility functions $\alpha(t)$, $\beta(t)$,

$$\begin{aligned}
\mu^{\mathrm{tt}}_{\alpha\mu} &= \alpha^{\mathrm{tt}} k_\alpha k_\mu + \beta^{\mathrm{tt}} (\delta_{\alpha\mu} - k_\alpha k_\mu) , \\
\mu^{\mathrm{tr}}_{\alpha\mu} &= \beta^{\mathrm{tr}} \varepsilon_{\alpha\mu\sigma} k_\sigma , \\
\mu^{\mathrm{td}}_{\alpha\mu\nu} &= \alpha^{\mathrm{td}} k_\alpha \overbrace{k_\mu k_\nu}^{(\mu\nu)} + \beta^{\mathrm{td}} \overbrace{(\delta_{\alpha\mu} - k_\alpha k_\mu) k_\nu}^{(\mu\nu)} , \\
\mu^{\mathrm{rt}}_{\alpha\mu} &= \beta^{\mathrm{rt}} \varepsilon_{\alpha\mu\sigma} k_\sigma , \\
\mu^{\mathrm{rr}}_{\alpha\mu} &= \alpha^{\mathrm{rr}} k_\alpha k_\mu + \beta^{\mathrm{rr}} (\delta_{\alpha\mu} - k_\alpha k_\mu) , \\
\mu^{\mathrm{rd}}_{\alpha\mu\nu} &= \beta^{\mathrm{rd}} k_\sigma \overbrace{\varepsilon_{\sigma\alpha\mu} k_\nu}^{(\mu\nu)} , \\
\mu^{\mathrm{dt}}_{\alpha\beta\mu} &= \alpha^{\mathrm{dt}} \overbrace{k_\alpha k_\beta}^{(\alpha\beta)} k_\mu + \beta^{\mathrm{dt}} \overbrace{k_\alpha (\delta_{\beta\mu} - k_\beta k_\mu)}^{(\alpha\beta)} , \\
\mu^{\mathrm{dr}}_{\alpha\beta\mu} &= \beta^{\mathrm{dr}} \overbrace{k_\alpha \varepsilon_{\beta\mu\sigma}}^{(\alpha\beta)} k_\sigma .
\end{aligned} \tag{71}$$

The symmetry properties (70) lead to the following identities for the scalar mobility functions:

$$\beta^{tr} = -\beta^{rt}, \qquad \alpha^{td} = -\alpha^{dt}, \qquad \beta^{td} = -\beta^{dt}, \qquad \beta^{rd} = \beta^{dr}. \tag{72}$$

Note that some signs in Eq. (72) differ from signs in corresponding relations in Eq. (49); this is because the full mobility matrix as defined in Eq. (68) is not the inverse of the full friction matrix defined in Eq. (31).

Just as for the friction functions in Eq. (51) it is convenient to introduce dimensionless mobility functions by

$$\begin{aligned}
&\tilde{\alpha}^{tt} = 6\pi\eta a\, \alpha^{tt}, \qquad \tilde{\beta}^{tt} = 6\pi\eta a\, \beta^{tt}, \\
&\tilde{\alpha}^{rr} = 8\pi\eta a^3\, \alpha^{rr}, \qquad \tilde{\beta}^{rr} = 8\pi\eta a^3\, \beta^{rr}, \\
&\tilde{\alpha}^{dt} = \alpha^{dt}/a, \qquad \tilde{\beta}^{dt} = \beta^{dt}/a, \\
&\tilde{\beta}^{tr} = 8\pi\eta a^2 \beta^{tr}, \qquad \tilde{\beta}^{dr} = \beta^{dr}.
\end{aligned} \tag{73}$$

The consistency of the definitions (31) and (68) leads to simple algebraic relations between the scalar functions $\tilde{\alpha}, \tilde{\beta}$ and the $\tilde{\phi}, \tilde{\psi}$. We find

$$\begin{aligned}
&\tilde{\alpha}^{tt} = 1/\tilde{\phi}^{tt}, \qquad \tilde{\beta}^{tt} = \tilde{\psi}^{rr}/[\tilde{\psi}^{tt}\tilde{\psi}^{rr} - \tfrac{4}{3}(\tilde{\psi}^{tr})^2], \\
&\tilde{\alpha}^{rr} = 1/\tilde{\phi}^{rr}, \qquad \tilde{\beta}^{rr} = \tilde{\psi}^{tt}/[\tilde{\psi}^{tt}\tilde{\psi}^{rr} - \tfrac{4}{3}(\tilde{\psi}^{tr})^2], \\
&\tilde{\beta}^{tr} = -\tilde{\psi}^{tr}/[\tfrac{3}{4}\tilde{\psi}^{tt}\tilde{\psi}^{rr} - (\tilde{\psi}^{tr})^2], \\
&\tilde{\alpha}^{dt} = -\tilde{\phi}^{dt}\tilde{\alpha}^{tt}, \qquad \tilde{\beta}^{dt} = -\tilde{\psi}^{dt}\tilde{\beta}^{tt} - \tilde{\psi}^{dr}\tilde{\beta}^{tr}, \\
&\tilde{\beta}^{dr} = -\tfrac{3}{4}\tilde{\psi}^{dt}\tilde{\beta}^{tr} - \tilde{\psi}^{dr}\tilde{\beta}^{rr}.
\end{aligned} \tag{74}$$

If we wish to determine the translational and angular velocities $\boldsymbol{U}$ and $\boldsymbol{\Omega}$ of a spherical particle acted on by external forces and torques $\mathscr{F}, \mathscr{T}$ and subject to an imposed flow field $\boldsymbol{v}_0$, we require the mobility matrix rather than the friction matrix. The scalar mobility functions α, β have reflection series expansions like those for the friction functions ϕ, ψ, but, as we have shown previously [25], these are less well-behaved than are the friction function series. For that reason, for the one particle problem considered here, it is computationally more efficient to calculate numerically the scalar friction functions as in Eq. (63) and then to obtain the mobility functions from the relations (73) and (74). This procedure is particularly useful in the near touching regime where the correct lubrication divergences of the ϕ, ψ, built into the representation (63), lead to accurate near touching mobilities.

Because of the singularities in the friction functions as $t \to 1$, many of the mobility functions vanish at touching. This means rather rapid changes in the mobility functions

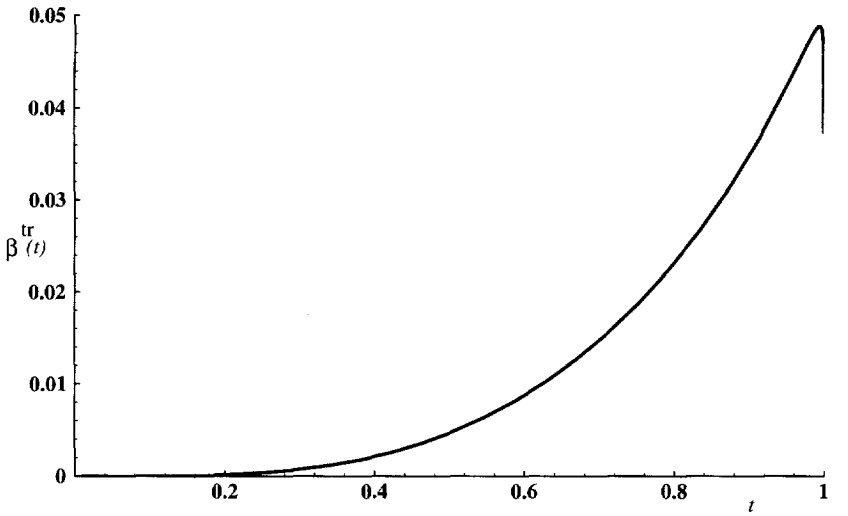


Fig. 5. Plot of the translation–rotation coupling mobility $\tilde{\beta}^{\mathrm{tr}}(t)$ for $0 \leqslant t \leqslant 1$. The last point plotted corresponds to $t = 0.99999$. Since this mobility vanishes at $t = 1$, there is rapid change very close to the wall.

in the range $0.9 \leqslant t \leqslant 1$. As $t \to 1$ we have the limiting behaviours

$$\begin{aligned} \tilde{\alpha}^{\mathrm{tt}} &\approx (1-t), \qquad \tilde{\beta}^{\mathrm{tt}} \approx -2[\ln(1-t)]^{-1}, \\ \tilde{\alpha}^{\mathrm{rr}} &\approx 1/\zeta(3), \qquad \tilde{\beta}^{\mathrm{rr}} \approx -\tfrac{8}{3}[\ln(1-t)]^{-1}, \\ \tilde{\alpha}^{\mathrm{dt}} &\approx 1, \qquad \tilde{\beta}^{\mathrm{dt}} \approx 2, \\ \tilde{\beta}^{\mathrm{tr}} &\approx -\tfrac{2}{3}[\ln(1-t)]^{-1}, \qquad \tilde{\beta}^{\mathrm{dr}} \approx 1. \end{aligned} \tag{75}$$

In Fig. 5 we plot $\tilde{\beta}^{\mathrm{tr}}(t)$ showing the rapid change of behaviour as $t \to 1$. Note that this function, which describes translation–rotation coupling is small for all values of t.

7. Falling sphere in shear flow

We conclude with a simple application of the results of earlier sections. We consider a hard sphere of mass density ρ suspended in a fluid of mass density ρ' subject to gravity and in the presence of an imposed shear flow of the form

$$\boldsymbol{v}_0(\boldsymbol{r}) = \gamma(0, z, 0) = \gamma z \hat{\boldsymbol{j}}. \tag{76}$$

The coordinate system is the same as that in Fig. 1 with the hard wall at $z = 0$. We suppose that there is no external torque acting on the particle but there will be a net gravitational force

$$\mathscr{F}_g = \tfrac{4}{3}\pi a^3(\rho - \rho')g\hat{\boldsymbol{G}} = \Delta m g(G_x, G_y, G_z), \tag{77}$$

where g is the acceleration due to gravity and the unit vector $\hat{\boldsymbol{G}}$ gives the direction of the buoyancy force. With a linear shear flow the vector $\boldsymbol{\omega}_0(\boldsymbol{R})$ and the rate of strain tensor $\boldsymbol{g}_0(\boldsymbol{R})$ defined in Eq. (33) take the forms

$$\boldsymbol{\omega}_0(\boldsymbol{R}) = \frac{\gamma}{2}(-1,0,0) = -\frac{\gamma}{2}\hat{\boldsymbol{i}}\,,$$

$$\boldsymbol{g}_0(\boldsymbol{R}) = \frac{\gamma}{2}\begin{pmatrix} 0 & 0 & 0 \\ 0 & 0 & 1 \\ 0 & 1 & 0 \end{pmatrix}. \tag{78}$$

Using the mobility matrix defined in Eq. (68) and remembering that with our assumptions above we have $\mathscr{F}_g = \mathscr{F}$ and $\mathscr{T} = 0$, we obtain the translational and angular velocities of the sphere with centre at $\boldsymbol{R}$ as

$$\boldsymbol{U}(\boldsymbol{R}) = \boldsymbol{v}_0(\boldsymbol{R}) + \boldsymbol{\mu}^{\mathrm{tt}} \cdot \mathscr{F}_g + \boldsymbol{\mu}^{\mathrm{td}} \cdot \boldsymbol{g}_0\,,$$

$$\boldsymbol{\Omega}(\boldsymbol{R}) = \boldsymbol{\omega}_0 + \boldsymbol{\mu}^{\mathrm{rt}} \cdot \mathscr{F}_g + \boldsymbol{\mu}^{\mathrm{rd}} \cdot \boldsymbol{g}_0\,. \tag{79}$$

Using Eqs. (71), (73) and (78) these equations become

$$\boldsymbol{U}(\boldsymbol{R}) = (U_g\,\tilde{\beta}^{\mathrm{tt}}(t)G_x, \frac{1}{t}U_s + U_g\,\tilde{\beta}^{\mathrm{tt}}(t)G_y + \tfrac{1}{2}U_s\,\tilde{\beta}^{\mathrm{td}}(t), U_g\,\tilde{\alpha}^{\mathrm{tt}}(t)G_z)\,, \tag{80}$$

and

$$\boldsymbol{\Omega}(\boldsymbol{R}) = (-\tfrac{1}{2}\gamma + \gamma_g\,\tilde{\beta}^{\mathrm{rt}}(t)G_y + \tfrac{1}{2}\gamma\,\tilde{\beta}^{\mathrm{rd}}(t), -\gamma\,\tilde{\beta}^{\mathrm{rt}}(t)G_x, 0)\,, \tag{81}$$

where

$$U_g = \frac{\Delta mg}{6\pi\eta a}, \qquad U_s = \gamma a, \qquad \gamma_g = \frac{\Delta mg}{8\pi\eta a^2}\,. \tag{82}$$

We can construct trajectories for the particle in position and orientation space by integrating the above equations. Denoting the time variable by τ, we define the position trajectory by $\boldsymbol{R}(\tau) = (X(\tau), Y(\tau), Z(\tau))$ remembering that the variable t, on which the mobility functions depend, is given by $t = a/h = a/Z$. The orientation trajectory is defined by a body-fixed coordinate frame moving with the sphere with unit vectors $\hat{\boldsymbol{n}}_i(\tau)$, $i = 1,2,3$. The trajectory equations are then

$$\frac{d\boldsymbol{R}}{d\tau} = \boldsymbol{U}(\boldsymbol{R}), \qquad \frac{d\hat{\boldsymbol{n}}_i}{d\tau} = \boldsymbol{\Omega}(\boldsymbol{R}) \times \hat{\boldsymbol{n}}_i\,. \tag{83}$$

The simplest case to consider is that when the gravitational field is normal to the wall, $\hat{\boldsymbol{G}} = (0,0,-1)$. The update equations simplify to

$$\frac{d\boldsymbol{R}}{d\tau} = \left(0, \frac{1}{t}U_s + \frac{1}{2}U_s\,\tilde{\beta}^{\mathrm{td}}(t), -U_g\,\tilde{\alpha}^{\mathrm{tt}}(t)\right),$$

$$\frac{d\hat{\boldsymbol{n}}_i}{d\tau} = \left(-\frac{1}{2}\gamma + \frac{1}{2}\gamma\,\tilde{\beta}^{\mathrm{rd}}(t), 0, 0\right) \times \hat{\boldsymbol{n}}_i\,. \tag{84}$$

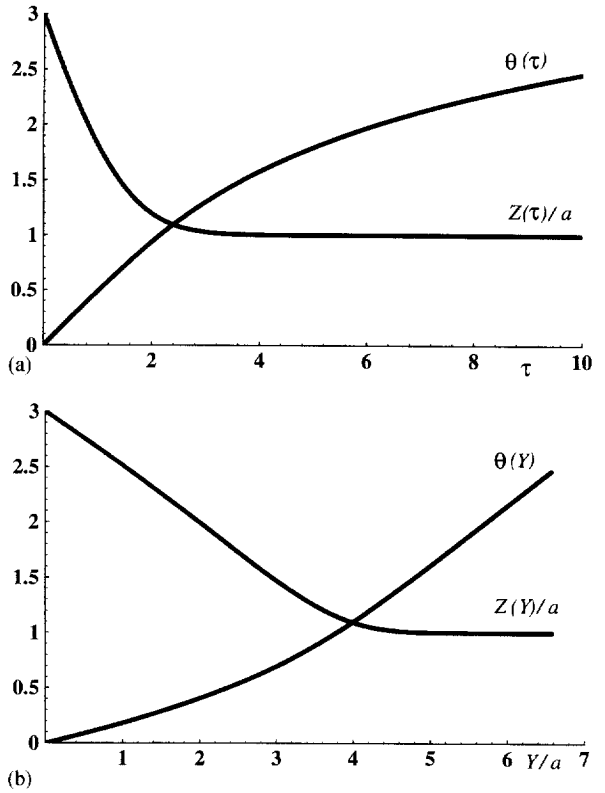


Fig. 6. In (a) we show, for a falling sphere in shear flow, the altitude above the wall, $Z(\tau)$, and the angle turned through, $\theta(\tau)$, as functions of time τ in seconds. In (b) we plot the same quantities as functions of Y, the horizontal distance travelled along the wall.

The differential equations (83) or (84) can be integrated numerically in a standard way using the accurate mobility functions given by Eqs. (63) and (74).

As an example, we have integrated (84) for the case of a sphere suspended in water, whose radius is $a = 10^{-6}$ m and whose density is twice that of water. The shear rate is taken to be $\gamma = 1\ \mathrm{s}^{-1}$. As initial conditions we take $\boldsymbol{R}(0) = (0, 0, 3a)$ with the body-fixed axes $\hat{\boldsymbol{n}}(0)$ taken parallel to the wall-fixed axes $\hat{\boldsymbol{i}}$, $\hat{\boldsymbol{j}}$, $\hat{\boldsymbol{k}}$. In this circumstance the sphere simply rotates about an axis through its centre parallel to $\hat{\boldsymbol{i}}$, the direction of the x-axis, so that its orientation is described by a single angle $\theta(\tau)$ which is the angle between $\hat{\boldsymbol{n}}_3(\tau)$ and $\hat{\boldsymbol{k}}$. In Fig. 6a we show $Z(\tau)/a$ and $\theta(\tau)$ plotted against time τ. In Fig. 6b we show the same two quantities, plotted this time as functions of Y, the lateral distance travelled along the wall. We see that $\theta(\tau)$ continues to change at a non-constant rate well after $Z(\tau)$ has essentially been frozen by the lubrication forces opposing motion towards the wall. This change in $\theta(\tau)$ reflects the strong position dependence of the mobility function $\tilde{\beta}^{\mathrm{rd}}$.

8. Discussion

The most important result of this paper is the description in Section 3 of the flow field around a single spherical particle near a hard wall in terms of fluid response to force multipoles on the actual sphere and on a mirror image sphere (22). This result is essential for treating the problem of many particles near a hard wall. Moreover, we have derived the result for a wide range of particle types, hard particles with stick or slip boundary conditions, droplets with high surface tension and porous particles. An immediate and powerful application of this result is to the calculation of the friction matrix for a single particle in the presence of a wall as explained in Sections 4 and 5. There we give an accurate representation of the friction functions (63) for all separations of particle and wall including the lubrication region. The asymptotic formulae given there correct misprints that have occurred elsewhere [17] and give new values for the constant terms in these asymptotic representations. In Section 6 we give the corresponding mobility functions including those describing coupling of the particle's translational and rotational motion to a linear shear flow. In Section 7 we show how the response of a single spherical particle to external forces may be studied by a Stokesian dynamics calculation of the particle trajectory. All of these results have a ready application to the Stokesian description of a many-particle system near a wall.

Acknowledgements

This research is partly funded by the United Kingdom EPSRC under grant GR/L49956.

Appendix A

Our purpose here is to outline briefly the derivation of identities used to establish the result (22) in Section 3. These identities concern the basis functions $\boldsymbol{v}^{+}_{lm\sigma}(\boldsymbol{s})$ used in the expansion of the Oseen tensor in Eq. (13). These functions are defined explicitly as [28]

$$\boldsymbol{v}^{+}_{lm0}(\boldsymbol{s}) = s^{l-1}\hat{\boldsymbol{A}}_{lm}(\hat{\boldsymbol{s}}),$$

$$\boldsymbol{v}^{-}_{lm1}(\boldsymbol{s}) = is^{l}\hat{\boldsymbol{C}}_{lm}(\hat{\boldsymbol{s}}),$$

$$\boldsymbol{v}^{+}_{lm2}(\boldsymbol{s}) = s^{l+1}\left(\frac{(l+1)(2l+3)}{2l}\hat{\boldsymbol{A}}_{lm}(\hat{\boldsymbol{s}}) + \hat{\boldsymbol{B}}_{lm}(\hat{\boldsymbol{s}})\right), \tag{A.1}$$

where the unit vector $\hat{\boldsymbol{s}}$ is given by $\hat{\boldsymbol{s}} = \boldsymbol{s}/s$ and $\hat{\boldsymbol{A}}_{lm}, \hat{\boldsymbol{B}}_{lm}, \hat{\boldsymbol{C}}_{lm}$ are unnormalized vector spherical harmonics related to the normalized vector harmonics $\boldsymbol{Y}_{JLM}$ of

Edmonds [40] by

$$\hat{\boldsymbol{A}}_{lm}(\hat{\boldsymbol{s}}) = n_{lm}\sqrt{l(2l+1)}\boldsymbol{Y}_{ll-1m}(\hat{\boldsymbol{s}}),$$
$$\hat{\boldsymbol{B}}_{lm}(\hat{\boldsymbol{s}}) = n_{lm}\sqrt{(l+1)(2l+1)}\boldsymbol{Y}_{ll+1m}(\hat{\boldsymbol{s}}),$$
$$\hat{\boldsymbol{C}}_{lm}(\hat{\boldsymbol{s}}) = -in_{lm}\sqrt{l(l+1)}\boldsymbol{Y}_{llm}(\hat{\boldsymbol{s}}). \tag{A.2}$$

The normalization constant n_{lm} is defined in Eq. (11). Edmonds defines the $\boldsymbol{Y}_{JLM}(\hat{\boldsymbol{s}})$ in terms of normalized scalar spherical harmonics $Y_{lm}(\hat{\boldsymbol{s}})$ and spherical basis vectors $\boldsymbol{e}_q$, $q=-1,0,1$, as

$$\boldsymbol{Y}_{JLM}(\hat{\boldsymbol{s}}) = \sum_{M'q'} Y_{LM'}(\hat{\boldsymbol{s}})\boldsymbol{e}_{q'}(LM'1q'|L1JM), \tag{A.3}$$

with appropriate Clebsch–Gordan coefficients $(LM'1q'|L1JM)$ [40]. The scalar harmonics $Y_{lm}(\hat{\boldsymbol{s}})$ may be written in terms of spherical polar coordinates θ,ϕ with polar axis taken normal to the wall in the direction $\hat{\boldsymbol{k}}$. It is easy to check from the definitions of $Y_{lm}(\hat{\boldsymbol{s}})$ and $\boldsymbol{e}_q$ that

$$\boldsymbol{P}\cdot\boldsymbol{e}_q = (-1)^{q+1}\boldsymbol{e}_q,$$
$$Y_{lm}(\boldsymbol{P}\cdot\hat{\boldsymbol{s}}) = Y_{lm}(\pi-\theta,\phi) = (-1)^{l+m}Y_{lm}(\theta,\phi) = (-1)^{l-m}Y_{lm}(\hat{\boldsymbol{s}}). \tag{A.4}$$

Remembering that the Clebsch–Gordan coefficient in Eq. (A.3) vanishes unless $M'+q'=M$, we find

$$\boldsymbol{P}\cdot\boldsymbol{Y}_{JLM}(\boldsymbol{P}\cdot\hat{\boldsymbol{s}}) = (-1)^{L+M+1}\boldsymbol{Y}_{JLM}(\hat{\boldsymbol{s}}). \tag{A.5}$$

It then follows from Eqs. (A.1) and (A.2) that

$$\boldsymbol{P}\cdot\boldsymbol{v}^{+}_{lm\sigma}(\boldsymbol{P}\cdot\boldsymbol{s}) = (-1)^{l+m+\sigma}\boldsymbol{v}^{+}_{lm\sigma}(\boldsymbol{s}). \tag{A.6}$$

In order to obtain the result (21) we use relations derived earlier [24,25]:

$$\boldsymbol{v}^{+}_{l_1m_1\sigma_1}(\boldsymbol{P}\cdot\boldsymbol{s}) = \sum_{l_2m_2\sigma_2} e(l_1m_1\sigma_1, l_2m_2\sigma_2)\boldsymbol{v}^{+}_{l_2m_2\sigma_2}(\boldsymbol{s}),$$

$$2\boldsymbol{v}^{+}_{l_1m_1\sigma_1}(\boldsymbol{s})\cdot\hat{\boldsymbol{k}}\hat{\boldsymbol{k}} = \sum_{l_2m_2\sigma_2} \Delta(l_1m_1\sigma_1, l_2m_2\sigma_2)\boldsymbol{v}^{+}_{l_2m_2\sigma_2}(\boldsymbol{s}),$$

$$(\hat{\boldsymbol{k}}\cdot\hat{\boldsymbol{s}})\boldsymbol{v}^{+}_{l_1m_1\sigma_1}(\boldsymbol{s}) = \cos\theta\,\boldsymbol{v}^{+}_{l_1m_1\sigma_1}(\boldsymbol{s})$$
$$= \sum_{l_2m_2\sigma_2} f(l_1m_1\sigma_1, l_2m_2\sigma_2)\boldsymbol{v}^{+}_{l_2m_2\sigma_2}(\boldsymbol{s}),$$

$$\sin^2\theta\frac{\partial}{\partial\cos\theta}\boldsymbol{v}^{+}_{l_1m_1\sigma_1}(\boldsymbol{s}) = \sum_{l_2m_2\sigma_2} g(l_1m_1\sigma_1, l_2m_2\sigma_2)\boldsymbol{v}^{+}_{l_2m_2\sigma_2}(\boldsymbol{s}). \tag{A.7}$$

The matrices e, Δ, f, g are diagonal in m_1, m_2 and their non-zero elements are given in Refs. [24,25]. In these papers the identities are written for a spherical surface of radius $s = a$ but they are valid for any radius s. There is a misprint in Eq. (A.10) of Ref. [24] where the element $e(lm1, lm1)$ should not contain a factor a^2. The identity (A.6) shows that the matrices e and Δ are not independent. We may write (A.6) in terms of e and δ as

$$\sum_{l_2 m_2 \sigma_2} (\delta_{l_1 l_2}\delta_{m_1 m_2}\delta_{\sigma_1 \sigma_2} - \Delta(l_1 m_1 \sigma_1, l_2 m_2 \sigma_2)) e(l_2 m_2 \sigma_2, l_3 m_3 \sigma_3)$$
$$= (-1)^{l_1 + m_1 + \sigma_1} \delta_{l_1 l_3}\delta_{m_1 m_3}\delta_{\sigma_1 \sigma_3} . \tag{A.8}$$

Noting that $\boldsymbol{P} \cdot \boldsymbol{P} = \mathbf{1}$, we see that the matrix e also satisfies, $e^2 = 1$. Using this observation together with Eq. (A.8) gives

$$\delta_{l_1 l_2}\delta_{m_1 m_2}\delta_{\sigma_1 \sigma_2} - \Delta(l_1 m_1 \sigma_1, l_2 m_2 \sigma_2) = (-1)^{l_1 + m_1 + \sigma_1} e(l_1 m_1 \sigma_1, l_2 m_2 \sigma_2) . \tag{A.9}$$

In Ref. [25] we have also the further differential identities

$$\nabla_s^2 \boldsymbol{v}_{lm0}^+(\boldsymbol{s}) = 0, \quad \nabla_s^2 \boldsymbol{v}_{lm1}^+(\boldsymbol{s}) = 0 ,$$
$$\nabla_s^2 \boldsymbol{v}_{lm2}^+(\boldsymbol{s}) = \frac{(l+1)(2l+1)(2l+3)}{l} \boldsymbol{v}_{lm0}^+(\boldsymbol{s}) , \tag{A.10}$$

where ∇_s^2 is the Laplacian with respect to the variable $\boldsymbol{s}$.

To establish the result (21) we must evaluate $\nabla_s(\hat{\boldsymbol{k}} \cdot \boldsymbol{v}_{lm\sigma}^+(\boldsymbol{s}))$. For this purpose it is useful also to represent the functions $\hat{\boldsymbol{A}}_{lm}, \hat{\boldsymbol{B}}_{lm}, \hat{\boldsymbol{C}}_{lm}$ as

$$\hat{\boldsymbol{A}}_{lm}(\hat{\boldsymbol{s}}) = s^{-l+1} \nabla_s (s^l \hat{Y}_{lm}(\hat{\boldsymbol{s}})) ,$$
$$\hat{\boldsymbol{B}}_{lm}(\hat{\boldsymbol{s}}) = s^{l+2} \nabla_s (s^{-l-1} \hat{Y}_{lm}(\hat{\boldsymbol{s}})) ,$$
$$\hat{\boldsymbol{C}}_{lm}(\hat{\boldsymbol{s}}) = -\boldsymbol{s} \times \nabla_s (\hat{Y}_{lm}(\hat{\boldsymbol{s}})) , \tag{A.11}$$

where $\hat{Y}_{lm}(\hat{\boldsymbol{s}})$ is an unnormalized scalar harmonic defined by

$$\hat{Y}_{lm}(\hat{\boldsymbol{s}}) = n_{lm} Y_{lm}(\hat{\boldsymbol{s}}) = (-1)^m P_l^m(\cos\theta) e^{im\phi} , \tag{A.12}$$

with P_l^m an associated Legendre function [40]. By use of the expression for $\hat{\boldsymbol{A}}_{lm}$ given in Eq. (A.11) it is straightforward to show that

$$\nabla_s(\hat{\boldsymbol{k}} \cdot \boldsymbol{v}_{lm0}^+(\boldsymbol{s})) = (\hat{\boldsymbol{k}} \cdot \nabla_s) \boldsymbol{v}_{lm0}^+(\boldsymbol{s}) = \left(\cos\theta \frac{\partial}{\partial s} + \frac{1}{s} \sin^2\theta \frac{\partial}{\partial \cos\theta} \right) \boldsymbol{v}_{lm0}^+(\boldsymbol{s}) . \tag{A.13}$$

The two terms on the right-hand side are readily evaluated using the identities (A.7) to give

$$\nabla_s(\hat{\boldsymbol{k}} \cdot \boldsymbol{v}_{lm0}^+(\boldsymbol{s})) = (l+m) \boldsymbol{v}_{l-1m0}^+(\boldsymbol{s}) . \tag{A.14}$$

Since $\boldsymbol{s} \times \nabla_s$ is the generator of rotations, it is easy to see that

$$\hat{\boldsymbol{k}} \cdot \boldsymbol{v}_{lm1}^+(\boldsymbol{s}) = -is^l \hat{\boldsymbol{k}} \cdot (\boldsymbol{s} \times \nabla_s) \hat{Y}_{lm}(\hat{\boldsymbol{s}}) = m s^l \hat{Y}_{lm}(\hat{\boldsymbol{s}}) , \tag{A.15}$$

so that

$$\nabla_s(\hat{\boldsymbol{k}}\cdot\boldsymbol{v}^+_{lm1}(\boldsymbol{s}))=m\boldsymbol{v}^+_{lm0}(\boldsymbol{s})\,. \tag{A.16}$$

For the field $\boldsymbol{v}^+_{lm2}(\boldsymbol{s})$ the calculation of $\nabla_s(\hat{\boldsymbol{k}}\cdot\boldsymbol{v}^+_{lm2}(\boldsymbol{s}))$ is more lengthy. Using the definition of $\boldsymbol{v}^+_{lm2}(\boldsymbol{s})$ in Eq. (A.1) together with Eq. (A.11) leads to the result

$$\begin{aligned}\hat{\boldsymbol{k}}\cdot\boldsymbol{v}^+_{lm2}(\boldsymbol{s}) &= -\frac{(2l+1)(2l+3)}{l}s_z s^l\hat{Y}_{lm}(\hat{\boldsymbol{s}})+\frac{(2l+1)(l+3)}{2l}\hat{\boldsymbol{k}}\cdot\nabla_s(s^{l+2}\hat{Y}_{lm}(\hat{\boldsymbol{s}}))\\ &=\frac{(2l+1)(l+1)}{2}s^{l+1}\cos\theta\hat{Y}_{lm}(\hat{\boldsymbol{s}})\\ &\quad+\frac{(2l+1)(l+3)}{2l}s^{l+1}\sin^2\theta\frac{\hat{c}}{\hat{c}\cos\theta}\hat{Y}_{lm}(\hat{\boldsymbol{s}})\,.\end{aligned} \tag{A.17}$$

Using simple identities for the associated Legendre functions [40] and the definition (A.12) we can re-express $\cos\theta P^m_l(\cos\theta)$ and $\sin^2\theta\frac{\hat{c}}{\hat{c}\cos\theta}P^m_l(\cos\theta)$ to obtain the alternative expression

$$\hat{\boldsymbol{k}}\cdot\boldsymbol{v}^+_{lm2}(\boldsymbol{s})=\frac{(l+1)(2l+3)(l+m)}{2l}s^{l+1}\hat{Y}_{l-1m}(\hat{\boldsymbol{s}})-(l-m+1)s^{l+1}\hat{Y}_{l+1m}(\hat{\boldsymbol{s}})\,. \tag{A.18}$$

Using Eq. (A.11) and then Eq. (A.1) again, we find

$$\begin{aligned}\nabla_s(\hat{\boldsymbol{k}}\cdot\boldsymbol{v}^+_{lm2}(\boldsymbol{s}))&=\frac{(l+1)(2l+1)(2l+3)(l+m)}{2l(l-1)}s^2\boldsymbol{v}^+_{l-1m0}(\boldsymbol{s})\\ &\quad-\frac{(l+1)(2l+3)(l+m)}{l(2l-1)}\boldsymbol{v}^+_{l-1m2}(\boldsymbol{s})-(l-m+1)\boldsymbol{v}^+_{l+1m0}(\boldsymbol{s})\,.\end{aligned} \tag{A.19}$$

Note finally that the factors of s_z and s_z^2 which occur in Eq. (21) may be handled by repeated use of the third identity in Eq. (A.7).

The above results mean that each piece of the left-hand side of Eq. (21) is a linear combination of the fields $\boldsymbol{v}^+_{lm\sigma}(\boldsymbol{s})$ with powers of s multiplying some terms. However, when these pieces are combined, all terms with powers of s as factors cancel, leaving a linear combination of the functions $\boldsymbol{v}^+_{lm\sigma}(\boldsymbol{s})$ with coefficients that depend only on h, the height of the sphere centre above the wall, and numerical factors. These coefficients are denoted $\mathscr{C}(h;l_1m_1\sigma_1,l_2m_2\sigma_2)$ in Eq. (21) and are used to define the matrix $\mathscr{R}$ in Eq. (24). The non-zero elements of $\mathscr{R}$ are as follows:

$$\mathscr{R}(h;lm0,l-2m2)=(-1)^{l+m+1}\frac{4(l-2)(l+m)(l+m-1)}{(l-1)(2l-1)(2l-3)}\,,$$

$$\mathscr{R}(h;lm0,l-1m0)=(-1)^{l+m+1}2h(l+m)\,,$$

$$\mathscr{R}(h;lm0,l-1m1)=-(-1)^{l-m+1}\frac{4m(l+m)}{l(l-1)}\,,$$

$$\mathscr{R}(h;lm0,lm0)=(-1)^{l+m+1}\left(1+\frac{2(l-2)(l+m)(l-m)}{l(2l-1)}\right)\,,$$

$$\mathscr{R}(h; lm1, l-1m2) = (-1)^{l+m}\frac{4(l-1)m(l+m)}{l(2l-1)(2l+1)},$$

$$\mathscr{R}(h; lm1, lm0) = (-1)^{l+m}2hm,$$

$$\mathscr{R}(h; lm1, lm1) = (-1)^{l+m}\left(1-\frac{4m^2}{l(l+1)}\right),$$

$$\mathscr{R}(h; lm1, l+1m0) = (-1)^{l+m}\frac{2(l-1)m(l-m+1)}{(l+1)(2l+1)},$$

$$\mathscr{R}(h; lm2, l-1m2) = -(-1)^{l+m+1}2h\frac{(l-1)(l+1)(2l+3)(l+m)}{l^2(2l-1)},$$

$$\mathscr{R}(h; lm2, lm0) = -(-1)^{l+m+1}h^2\frac{(l+1)(2l+1)(2l+3)}{l},$$

$$\mathscr{R}(h; lm2, lm1) = (-1)^{l+m+1}2h\frac{m(2l+1)(2l+3)}{l^2},$$

$$\mathscr{R}(h; lm2, lm2) = (-1)^{l+m+1}\left(1-\frac{2(l+3)(l-m+1)(l+m+1)}{(l+1)(2l+3)}\right),$$

$$\mathscr{R}(h; lm2, l+1m0) = -(-1)^{l+m+1}4h(l+2)(l-m+1),$$

$$\mathscr{R}(h; lm2, l+1m1) = (-1)^{l-m+1}\frac{2m(l+3)(2l+1)(l-m+1)}{l(l+1)(l+2)},$$

$$\mathscr{R}(h; lm2, l+2m0) = -(-1)^{l+m+1}\frac{(l+3)(2l+1)(l-m+1)(l-m+2)}{(l+2)(2l+3)}.$$

(A.20)

References

[1] P.N. Pusey, in: J.P. Hansen, D. Levesque, J. Zinn-Justin (Eds.), Liquids, Freezing and Glass Transition, North-Holland, Amsterdam, 1991.

[2] R.B. Jones, P.N. Pusey, Annu. Rev. Phys. Chem. 42 (1991) 137.

[3] W.B. Russel, D.A. Saville, W.R. Schowalter, Colloidal Dispersions, Cambridge University Press, Cambridge, 1989.

[4] J.K.G. Dhont, An Introduction to Dynamics of Colloids, Elsevier Science, Amsterdam, 1996.

[5] G. Nägele, Phys. Rep. 272 (1996) 215.

[6] S. Kim, S.J. Karrila, Microhydrodynamics: Principles and Selected Applications, Butterworth-Heinemann, Boston, 1991.

[7] L. Durlofsky, J.F. Brady, G. Bossis, J. Fluid Mech. 180 (1987) 21.

[8] A.J.C. Ladd, J. Chem. Phys. 88 (1988) 5051; 90 (1989) 1149; 93 (1990) 3484; Phys. Fluids A 92 (1993) 299.

[9] B. Cichocki, B.U. Felderhof, K. Hinsen, E. Wajnryb, J. Blawzdziewicz, J. Chem. Phys. 100 (1994) 3780.

[10] N. Ostrowsky, L. Lobry, Il Nuovo Cimento 16D (1994) 1111.

[11] J.Y. Walz, L. Suresh, J. Chem. Phys. 103 (1995) 10714.

[12] C.W.J. Beenakker, P. Mazur, Phys. Fluids 28 (1985) 767, 3203.

[13] D. Leighton, A. Acrivos, Chem. Eng. Sci. 41 (1986) 1377; J. Fluid. Mech. 177 (1987) 109; 181 (1987) 415.

[14] A.T. Clark, M. Lal, G.M. Watson, Faraday Discuss. Chem. Soc. 83 (1987) 179.

[15] I. Pagonabarraga, P. Wojtaszczyk, J.M. Rubi, B. Senger, J.-C. Voegel, P. Schaaf, J. Chem. Phys. 105 (1996) 7815.

[16] H.A. Lorentz, Versl. Kon. Akad. Wetensch. Amsterdam 5 (1896) 168.
[17] G. Bossis, A. Meunier, J.D. Sherwood, Phys. Fluids A 3 (1991) 1853.
[18] R.G. Cox, H. Brenner, J. Fluid Mech. 28 (1967) 391.
[19] P. Mazur, D. Bedeaux, Physica 76 (1974) 235.
[20] B.U. Felderhof, Physica A 84 (1976) 557, 569.
[21] R.B. Jones, R. Schmitz, Physica A 149 (1988) 373.
[22] R. Schmitz, B.U. Felderhof, Physica A 113 (1982) 90.
[23] J. Happel, H. Brenner, Low Reynolds Number Hydrodynamics, Noordhoff, Leiden, 1973, p. 85.
[24] G. Perkins, R.B. Jones, Physica A 171 (1991) 575.
[25] G. Perkins, R.B. Jones, Physica A 189 (1992) 447.
[26] R.B. Jones, B.U. Felderhof, J.M. Deutch, Macromolecules 8 (1975) 680.
[27] J.R. Blake, Proc. Cambridge. Phil. Soc. 70 (1971) 303.
[28] B. Cichocki, B.U. Felderhof, R. Schmitz, Phys. Chem. Hydrodyn. 10 (1988) 383.
[29] H. Lamb, Hydrodynamics, 6th ed., Cambridge University Press, Cambridge, 1932.
[30] B.U. Felderhof, R.B. Jones, J. Math. Phys. 30 (1989) 339.
[31] W.R. Dean, M.E. O'Neill, Mathematika 10 (1963) 13.
[32] M.E. O'Neill, Mathematika 11 (1964) 67.
[33] M.E. O'Neill, K. Stewartson, J. Fluid Mech. 27 (1967) 705.
[34] R.G. Cox, H. Brenner, Chem. Eng. Sci. 22 (1967) 1753.
[35] A.J. Goldman, R.G. Cox, H. Brenner, Chem. Eng. Sci. 22 (1967) 637.
[36] A.J. Goldman, R.G. Cox, H. Brenner, Chem. Eng. Sci. 22 (1967) 653.
[37] D.J. Jeffrey, Y. Onishi, J. Fluid Mech. 139 (1984) 261.
[38] R.M. Corless, D.J. Jeffrey, J. Appl. Math. Phys. (ZAMP) 39 (1988) 874.
[39] G.A. Baker, P. Graves-Morris, Padé Approximants, in: G.-C. Rota (Ed.), Encyclopedia of Mathematics and its Applications, vol. 13, Addison-Wesley, Reading, MA, 1981.
[40] A.R. Edmonds, Angular Momentum in Quantum Mechanics, Princeton Univ. Press, Princeton, NJ, 1957.